Progress in Retinal and Eye Research 37 (2013) 141–162

Contents lists available at ScienceDirect

Progress in Retinal and Eye Research

journal homepage: www.elsevier.com/locate/prer

Retinal connectomics: Towards complete, accurate networks☆

Robert E. Marc*, [1], Bryan W. Jones [1], Carl B. Watt [1], James R. Anderson [1], Crystal Sigulinsky [1], Scott Lauritzen [1]

University of Utah School of Medicine, Department of Ophthalmology, John A. Moran Eye Center, 65 Mario Capecchi Dr, Salt Lake City, UT 84132, USA

ARTICLE INFO

Article history:
Available online 7 September 2013

Keywords:
Retina
Neurons
Connectome
Networks
Synapses
Gap junctions

ABSTRACT

Connectomics is a strategy for mapping complex neural networks based on high-speed automated electron optical imaging, computational assembly of neural data volumes, web-based navigational tools to explore 10^{12}–10^{15} byte (terabyte to petabyte) image volumes, and annotation and markup tools to convert images into rich networks with cellular metadata. These collections of network data and associated metadata, analyzed using tools from graph theory and classification theory, can be merged with classical systems theory, giving a more completely parameterized view of how biologic information processing systems are implemented in retina and brain. Networks have two separable features: topology and connection attributes. The first findings from connectomics strongly validate the idea that the topologies of complete retinal networks are far more complex than the simple schematics that emerged from classical anatomy. In particular, connectomics has permitted an aggressive refactoring of the retinal inner plexiform layer, demonstrating that network function cannot be simply inferred from stratification; exposing the complex geometric rules for inserting different cells into a shared network; revealing unexpected bidirectional signaling pathways between mammalian rod and cone systems; documenting selective feedforward systems, novel candidate signaling architectures, new coupling motifs, and the highly complex architecture of the mammalian A_{II} amacrine cell. This is but the beginning, as the underlying principles of connectomics are readily transferrable to non-neural cell complexes and provide new contexts for assessing intercellular communication.

Contents

* Corresponding author. Tel.: +1 801 585 6500; fax: +1 801 587 7724.
E-mail addresses: robert.marc@hsc.utah.edu (R.E. Marc), bryan.jones@m.cc.utah.edu (B.W. Jones), carl.watt@hsc.utah.edu (C.B. Watt), James.R.Anderson@utah.edu (J.R. Anderson), jscottlauritzen@gmail.com (C. Sigulinsky), jscottlauritzen@gmail.com (S. Lauritzen).

[1] Percentage of work contributed by each author in the production of the manuscript is as follows: Marc, 40%; Jones, 10%; Watt, 10%; Anderson, 15%; Lauritzen, 25%.

1350-9462/$ – see front matter © 2013 The Authors. Published by Elsevier Ltd. All rights reserved.
http://dx.doi.org/10.1016/j.preteyeres.2013.08.002

1. Connectomics

A new field like connectomics brings with it much uncertainty, contention and new terminologies. The uncertainly derives in part from the fact that connectomics blends new methods (fast electron optical imaging, image processing algorithms, dataset assembly methods, database architectures, hardware configurations) and new interpretive frameworks (graph theory, computational complexity theory, classification theory). Contention arises in part from concerns that claims of improved network analysis may be overstated; that discovery may not reasonably scale with cost; and that some theoretical underpinnings are disputed.

As the field is not mature, many neuroscientists have opinions on its merits and how its discourses ought to be framed. A recent issue of Nature Methods (Volume 10, No 6, June 2013) contains many of these debates and they are not repeated here except to note that the arguments for and against connectomics are elegantly summarized by Morgan and Lichtman (2013). However, this review is not nor is it intended to be balanced. Rather it presents our experience with connectomics technology and discovery. Finally, graph theory, classification theory, electron optics and computational management of large datasets all involve unfamiliar conceptual frameworks and terminologies. This review is not intended to remedy understanding of all those areas, but will provide directions to the primary literature, textbooks and technical overviews. The review formally ends at Section 3. Sections 4.1–4.3 provides a detailed list of critical definitions and references. We encourage the reader to refer to them as needed. Sections 4.5 and 4.6 provide deeper explorations of network theory and classification forming the underpinning of modern connectomics, including arguments supporting the essential role of connectomics in achieving complete understanding of retinal networks.

1.1. Introduction

A connectome is a complete graph of a neural network. In principle, it is not an approximation or even a statistical average. It is a comprehensive list of every connection in a defined neural region. In practice, no studies have achieved this completeness, but unlike previous anatomical efforts, the goal is clear and the technical path straightforward. We expect completeness from community efforts, not from one lab. Connectomics efforts include macroscalestudies of connectivity across the brain (Marcus et al., 2011; Sporns et al., 2005; van den Heuvel and Sporns, 2011), mesoscale optical studies of connections between defined brain regions (Kleinfeld et al., 2011; Oberlaender et al., 2011), as well as nanoscale electron optical studies of synaptic connectivity, e.g. the vertebrate retina (Anderson et al., 2011b; Briggman et al., 2011). Fine-scale, ultrastructural connectome assembly has become possible due to high-speed automated electron optical imaging, including scanning electron microscope (SEM) and transmission electron microscope (TEM) imaging. Connectome analysis has become possible due to the development of large-scale annotation and database mining tools such as Viking and Connectome Viz (Anderson et al., 2011a).

1.2. Connectomics versus legacy anatomy

Why do we need a new approach to ultrastructural connectivity analysis at all? Don't we already know all the fundamental networks of retina? The answer to that is: No (Marc et al., 2012a; Anderson et al., 2011a: Lauritzen et al., 2012a,b; Briggman et al., 2011). We do not even really know if we have classified all retinal neurons, including bipolar, amacrine and ganglion cells and it is clear from new cell-specific genetic techniques that even well-known cells may have surprising roles in vision (Beier et al., 2013; Huberman and Niell, 2011; Rivlin-Etzion et al., 2011). So what is wrong with legacy analyses using traditional electron microscopy? Basically, legacy anatomy is ponderously slow and limited by the capacity of a single human observer to select and capture an image. Given the proliferation of new genetic models and new understanding of pathologic rewiring in the retina (Jones et al., 2011, 2003), high throughput ultrastructure is an essential advance. Previous TEM montaging efforts produced only arrays of single images for humans to track as stacks of photographs or low resolution digital files. For neuroscience, this meant that legacy ultrastructural anatomy, which (albeit heroic in scope) actually delivered only a broad-brush concepts and only fragments of retinal networks at best (Calkins and Sterling, 1996, 2007; Calkins

et al., 1998; Klug et al., 2003; Kolb and Famiglietti, 1974b; Kolb and Nelson, 1993; Stevens et al., 1980; Strettoi et al., 1992). That said, these studies discovered the baseline network for understanding signal flow in the retina. TEM studies of A_{II} amacrine cells (ACs) described an architecture that still cannot be explained by or predicted from physiological data. However, none of these original TEM data have been accessioned, in contrast to genetic data. From the user perspective, previous ultrastructure resembles fine art: a collection of uncurated, low-resolution halftone journal images, with no primary data or metadata available. Connectomics changes that by allowing public access to all raw and processed TEM data as well as metadata.

2. Creating connectomes

2.1. Connectome samples

Connectomics samples use conventional TEM fixation with mixed aldehydes, osmium e*n bloc* staining and optional *en bloc* uranyl acetate for electron imaging. The optimal method at present uses conventional glutaraldehyde fixation, e.g. many Karnovsky's variants, with light osmium post-staining. A variety of methods can be used to enhance TEM contrast for digital capture, such as ferrocyanide staining, but caution needs to be used. Such methods function by depositing metal atoms (e.g. osmium, iron) on the surfaces of endogenous proteins, lipids and DNA and these atoms occlude antibody access for immunocytochemistry. Only removal of osmium is technically feasible at present and even that requires delicate management of oxidative deosmication. Iron cannot be removed without extensive sample damage. As one key goal in connectomics is the fusion of TEM and small molecule immunocytochemistry targeting endogenous signals (Marc and Liu, 2000) or exogenous probes such as the channel permeant organic ion 1-amino-4-guanidobutane (AGB) (Anderson et al., 2011b, 2009), we avoid use of ferrocyanide. Briggman et al. (2011) and Bock et al. (2011) fused optical calcium imaging with ultrastructure to identify neuronal subsets. New genetic markers that produce electron dense deposits, essentially a TEM "GFP" are now available (Gaietta et al., 2002; Hoffmann et al., 2010; Lichtman and Smith, 2008; Shu et al., 2011). In any case, complete connectomics requires molecular markers (Anderson et al., 2011b, 2009; Jones et al., 2011; Jones et al., 2003; Marc and Liu, 2000; Micheva and Bruchez, 2011; Micheva et al., 2010; Micheva and Smith, 2007).

Arguably each connectomics group has cogent reasons for using different imaging platforms and comparisons of performance have been published (Anderson et al., 2009). Our reasons for using ATEM are simple. It requires no new hardware. ATEM is, by far, the highest resolution technology available and is the only method that can unambiguously map and measure all synapses and gap junctions. It is the only flexible re-imaging technology. Finally, it is the only technology proven to be compatible with intrinsic molecular markers.

2.2. Connectome sectioning

The next step in connectomics is serial sectioning. There are three basic technologies under exploration at present. Ablation methods use either physical sectioning with an automated microtome, such as *in vacuo* serial block-face (SBF) sectioning (Briggman and Denk, 2006; Denk and Horstmann, 2004), or surface ablation via *in vacuo* ion beam milling (Knott et al., 2008), followed by scanning electron microscope (SEM) or scanning TEM (STEM) imaging of secondary electrons (surface-backscattered electrons). Ablation techniques require very thin sections since secondary electrons are essentially surface reflections of the sample. However, both SEM and STEM have limited resolution because the electron beam size can only be reduced to nanometer scale widths, and acquisition times can be quite long for large sample fields. Ablation methods are also incompatible with molecular markers, so far. However, these are superb methods for wide-field connectomics. Their biggest limitation has been their relatively poor lateral resolution which prevents reliable visualization of gap junctions and validated quantitation of synapses.

Manual ultramicrotomy using existing equipment is a viable option to an expensive specialized platform such as an ablation system (Anderson et al., 2011b, 2009; Bourne and Harris, 2011). Human microtomists can produce serial sections ranging from hundreds to thousands with minimal error far faster than TEM acquisition time. Sections are placed on standard low electron-contrast monomolecular films, followed by conventional staining and automated TEM (ATEM) imaging (Anderson et al., 2011b, 2009). Primary electron projection images of sections, optimally 50–70 nm thick, form images that can be used as 2D pages in a 3D volume, or even assembled as true 3D datasets. We typically place 1–3 sections on a grid to maximize the security of a series during grid handling (staining, storing, retrieving, imaging, restoring them to storage). In addition, intercalated thin sections are placed on slides for computational molecular phenotyping every 20–30 TEM sections, permitting the insertion of molecular data into the connectome (Figs. 1 and 2).

Automated sectioning onto electron dense Kapton® films has also been developed for STEM imaging (Kleinfeld et al., 2011). Hopefully that technology will advance to the point of enabling more efficient use of existing TEMs by using electron-transparent films. At present the approach appears too expensive for widespread adoption. SBF and ion beam milling enable preregistration of image fields, which is a nontrivial but achievable computational operation (Tasdizen et al., 2010) that manual sectioning and imaging requires.

2.3. ATEM imaging

Each slice of a connectome volume is composed of >1000 image tiles (Figs. 2 and 3) and total image storage for datasets (Anderson et al., 2011a, 2011b, 2009) can range from ≈10 terabytes (Tb) to >1000 Tb. This means that live display of connectomes must span large arrays of data drives. The size of a dataset is defined by a canonical field or volume (Anderson et al., 2011b, 2009) and by the resolution required to detect critical features such as gap junctions and synapses. In practice, this sets the resolution at 2 nm, not 10 nm as suggested by Kleinfeld et al. (2011). We selected 2 nm explicitly because it allows mapping all retinal cells and all their synapses (Anderson et al., 2009). But, even with 2 nm resolution, validation of some gap junctions and quantitation of small synapses still demands high resolution re-imaging (e.g. 0.3 nm), often with goniometric tilt. Only TEM can currently deliver this performance. Sections are imaged in a grid pattern with roughly 15% edge overlap using a JEOL JEM 1400 TEM and a Gatan Ultrascan phosphor-imaging camera (Anderson et al., 2011a, 2011b, 2009). In the rabbit retinal connectome RC1 (Anderson et al., 2011b) each image slice (the digital transform of a physical section) contains a canonical field of 0.243 mm diameter and, at a resolution of 2.18 nm/pixel, and requires 950–1100 individual images. The process of automating stage motion, focus and image capture is achieved by SerialEM, developed by David Mastronarde at the University of Colorado, Boulder (Mastronarde, 2005). A more advanced TEM system based on custom camera arrays and modified TEM column placement has been developed by Bock et al. (2011). This platform may be an ideal schema for future connectomics programs but will

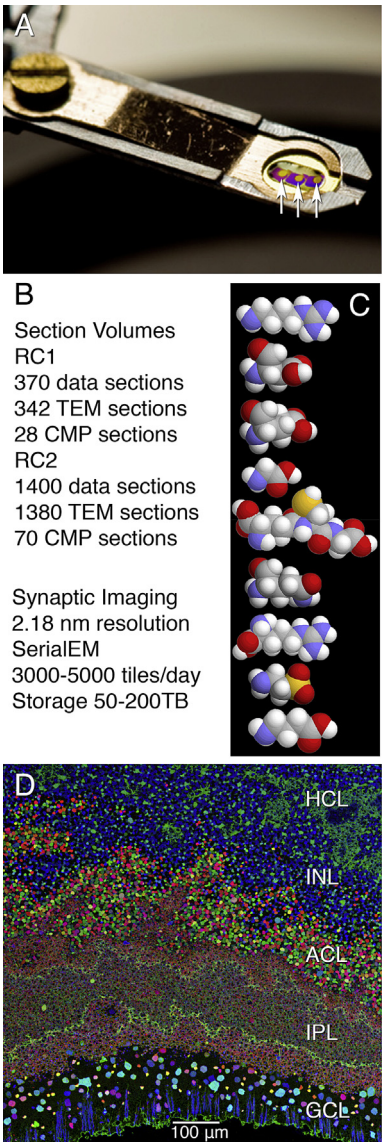

Fig. 1. Key aspects of high-resolution connectomes. (A) Small sets of serial TEM sections. The gold spots (arrows) are imaged connectome volume slices. (B) Parameters of connectomes RC1 and RC2. (C) Small molecules targeted by CMP. Top to bottom: AGB, aspartate, glutamate, glycine, glutathione, glutamine, arginine, taurine, GABA. (D) CMP imaging of GABA (red), AMPA-activated AGB (green), and glutamate (blue) in an oblique section of rabbit retina.

need a commercialization path, as it is not currently as readily implemented as SerialEM on existing TEM platforms.

2.4. Connectome assembly

There are two approaches for building navigable volumes. One converts 2D data slices into a 3D projections which, while useful if implemented at high resolution, requires high performance visualization environments many users lack. Others have opted for a paged architecture, similar to Google Earth and KML (Google, 2010), treating each slice as a single array of 2D mapped tiles in image pyramid form, which decreases computational overhead and facilitates navigation, access and sharing (Anderson et al., 2011a). Algorithms for automated tiling and slice-to-slice registrations (Tasdizen et al., 2010) use image Fourier shift to rapidly compute displacement vectors. Refined slice-to-slice alignments then automatically build

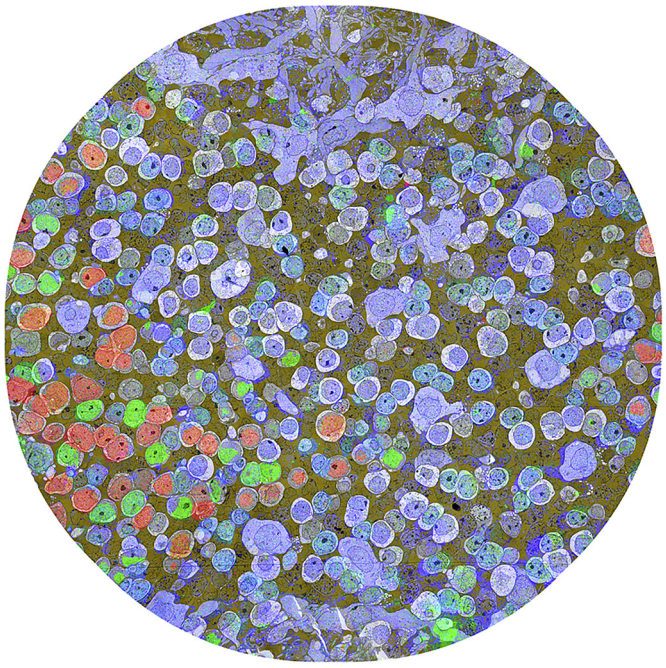

Fig. 2. Connectome RC1 slice 001. Composed of >1000 high-resolution TEM tiles, the slice is augmented with a transparency mapping simultaneously displaying GABA (red), glycine (green), glutamate (blue), and the logical AND of glutamine and taurine signals as a dark gold alpha channel. GABA+ (red) neurons are ACs, while glycine+ (green) neurons are either ACs or an ON cone BC subset. Glutamate+ (blue) neurons are largely BCs. Image width, 243 µm. From Anderson et al. (2011b), Molecular Vision 17:355–379 by permission of the authors.

2 nm resolution volumes. Similar approaches can also be used to align large scale optical atlases (Berlanga et al., 2011).

A physical connectome can be various sizes depending the resolution needed, the spatial scale of the canonical region required, and acquisition parameters. The limit on connectome size

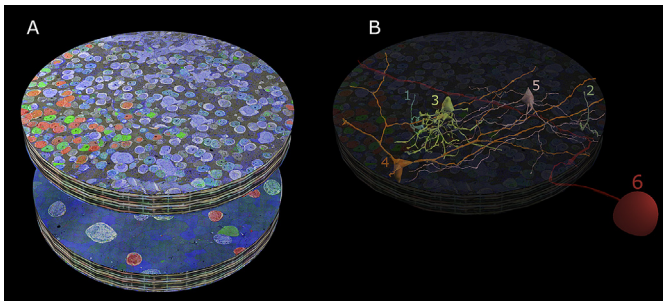

Fig. 3. RC1 volume overview. (A) The RC1 volume with its top section beginning in mid-INL and ending in the GCL shown in a mirror image. RC1 is a short cylinder ≈ 250 µm in diameter and ≈30 µm high containing 341 TEM sections and 11 intercalated CMP sections. The cylinder is capped at top and bottom with 10- section CMP series allowing molecular segmentation. TEM Section 001 is a near-horizontal plane section through the INL visualized with GABA.glycine.glutamate → red.green.blue transparency mapping and a dark gold alpha channel (ANDed taurine + glutamine channels) described in Anderson et al., (2011a). Similarly TEM section 371 is a near-horizontal plane section through the GCL visualized with GABA.AGB.glutamate → red.green.blue transparency mapping. (B) Representative cells contained in RC1 are rendered in 3D onto the volume. Many complete copies of small cells exist (tens to hundreds) such as rod BCs (cells 1,2) and A_{II} ACs (cell 3). A few semi-complete copies (5–10) of medium-diameter cell classes have their somas and much of their arbors within RC1, but extend outside it, such as interstitial γACs (cell 4) and A_I ACs (cell 5). Finally, RC1 contains many processes from partial cells: large cells such as wide-field ACs or OFF α GCs (cell 6) with somas outside the volume and often fully traversing it. From Lauritzen et al., (2012a,b), by permission of the authors.

is currently determined by the time required to image it at the chosen resolution. Imaging time is inversely proportional to the square of resolution. In the case of RC1, based on the rabbit inner plexiform layer, 2 nm resolution and a canonical somatic volume (one that contains at least one soma of every cell type) defined as a 0.243 mm cylinder spanning the inner nuclear and ganglion cell layers, acquisition required 5 months of TEM beam time and required 16.4 Tb of raw and ≈64 Tb total storage, including live data, a mirror, and archival backup. The volume contains over 300 bipolar cells (BCs), 300 Müller cells (MCs), 39 A_{II} ACs, over 100 ACs, and 20 ganglion cells (GCs) and includes a full set of small molecule markers for classification. Every cell can be reconstructed. However, this somatic volume is much smaller than a canonical dendritic volume in the rabbit retina (Fig. 3). The diameters of the largest GCs and ACs exceed 1 mm and full dendritic reconstructions with current technologies based on a single TEM would require 4–5 years of imaging time and a petabyte of storage, beyond any laboratory's current resources. A new strategy for this is a multiresolution approach, e.g. mixed 10 nm and 2 nm TEM imaging, with 10 nm captures being 25× faster. A new ATEM mouse retinal connectome spanning the outer nuclear and ganglion cell layers at a diameter of 0.28 mm is now being built. A stick figure of mouse inner plexiform layer connectome spanning about 0.08 mm × 0.1 mm has been published by Helmstaedter et al. (2013) that defines many mouse bipolar, amacrine and ganglion cell classes based on stratification, patterning and presumed contacts. It employs autodetection of synapses, but no ground truth data were published with it to validate those synapses, and no gap junctions were reported. Interestingly, ON and OFF bipolar cells were classified by stratification (Helmstaedter et al., 2013) rather than direct synaptic or gap junction contacts with A_{II} ACs (Anderson et al., 2011b; Lauritzen et al., 2012a, 2012b).

2.5. Navigating and mining connectomes

Conventional imaging tools are incapable of visualizing datasets as large as a connectome, much less navigating them in a structured way. New tools are required (Anderson et al., 2011a; Fiala, 2005; Helmstaedter et al., 2013; Jeong et al., 2010). By using image pyramid sets (Anderson et al., 2011a; Mikula et al., 2007), web-applications can readily view, transform and annotate connectomes. Anderson and colleagues have developed Viking, an open-source web-compliant environment (Anderson et al., 2011a) that allows visualization by converting datasets to web-optimized tiles, delivering volume transforms to client devices, and providing groups of users with connectome data simultaneously via conventional internet connections. By enabling rapid disc-based annotation, Viking converts raw ultrastructural data into rich network graphs (Fig. 4), 3D navigational skeletons, marks up synapses and other cellular identifiers, builds databases to be queried, and 3D renderings in multiple formats all at 2 nm or resolution. Presynaptic ribbons, patterned densities, vesicle clouds, postsynaptic densities, gap junctions, adherens junctions are characterized by their connectome physical locations, dimensions and parent structures, allowing the assembly of formal adjacency matrices.

Connectomics data are so difficult and expensive to acquire that, ethically they must be shared (Amari et al., 2002; Anderson et al., 2011a; Jeong et al., 2010; Marc et al., 2012a). Computational frameworks based on REST (REpresentational State Transfer)-compliant web-services (e.g. Viking) overcome the impracticality of distributing raw datasets. The Viking approach also uses common file formats to enable use of other visualization systems, e.g. Blender (www.blender.org) or Autodesk® Maya. Such approaches also minimize journal overhead costs since they needn't act as data

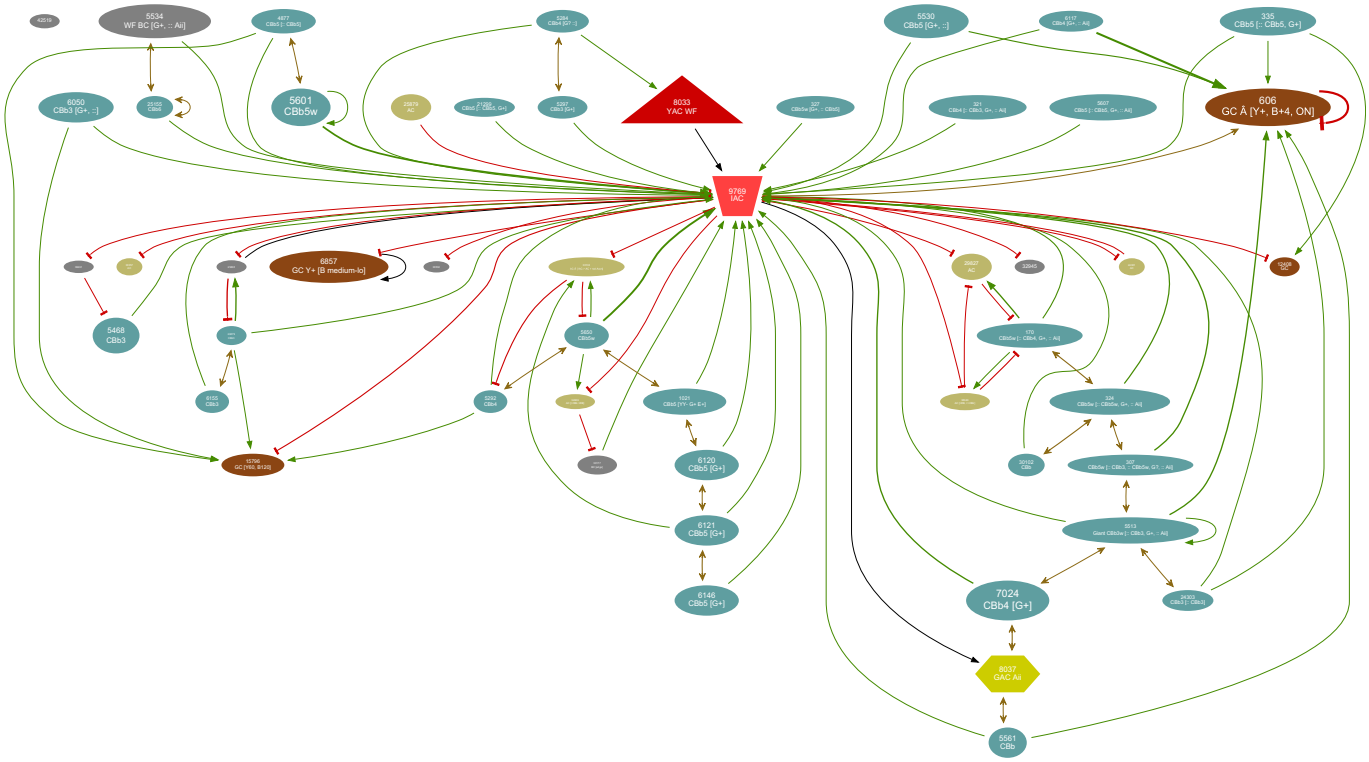

Fig. 4. A Connectome Viz graph. The one-hop graph of interstitial AC 9769 (the inverted trapezoid at the center of the image) built automatically from annotations in rabbit retinal volume RC1. Aqua ovals are ON cone BCs (CBb) presynaptic to cell 9769. The red triangle is a γAC presynaptic to 9769, the gold ovals are beaded-process γACs both pre- and postsynaptic to 9769, while the three brown ovals are GCs postsynaptic to 9769. Gray ovals are identified but unclassified cells. Green arrows are ribbon synapses, red bars are inhibitory synapses, gold two-headed arrows are gap junctions. Black arrows are adherens junctions.

repositories. We have opted for full public sharing of dataset RC1 and our tools. Connectomics enables a new generation of anatomical analyses: any cell can be traced many times, traced concurrently, with complete tracking of metadata. At any arbitrary origin in a data volume, a collection of synapses can be traced back to their sources while the physical locations and links (associations) for every cell or subcellular part are assembled into 3D renderings, network graphs, and navigational tools such as Viking Bookmarks, which are organized xml collections of locations, links, parent and child structures that can be used to support or illustrate any topic, hypothesis or analysis for a volume. Unlike classic legacy anatomy, everything done in connectomics is open and transparent. All the data and resources for the RC1 connectome are available through http://prometheus.med.utah.edu/~marclab.

3. Connectomics discovery

3.1. Introduction

The massive effort in developing connectomics technologies would be quixotic had there not been reasonable expectation of new and meaningful discoveries rather than just incremental validation of previous ideas of network architecture. Our earliest investigations have not only born out the idea that it was worth developing more complete network models, but have also shown that many retinal networks are more complex and diverse than expected. Furthermore, new signal flow paths have been found. In discussing these networks we use a set of typographic notations to compactly represent anatomically and physiologically diverse synaptic chains (see Section 4.6: Network Notation). These notations address the need to eventually go beyond adjacency matrices to weighted matrices. While physiological assessments for this parameterization do not exist for all aspects of the networks we are mapping, it is important to specify what those parameters might be and provide a database notation for them, even if we cannot model them completely. A seeming esoteric but nontrivial point is that these placeholder parameters (which now only hold simple values such as nominal polarity, approximate gain, presynaptic vesicle cloud size, postsynaptic density size, synapse numbers) are extensible vectors that can accommodate further complexity such as receptor type, voltage and time dependencies, modulation etc., as we learn how to acquire those features from coordinated connectomics/high throughput physiology studies in the future.

There are ten major areas in which connectomics is changing our understanding of cellular networks: Refactoring the inner plexiform layer via ON cone BC drive in the OFF layer, refactoring the inner plexiform layer via OFF cone BC drive in the ON layer, rod-cone crossover suppression, generalized crossover, tiered coupling, heterocellular coupling, sparse networks, joint distributions, nested AC networks, novel connection architectures. While it is beyond the scope of this paper, a broader ultrastructural analysis can be conceived: histomics, the quantitative analysis of heterocellular geometries in complex non-neuronal tissues.

3.2. ON cone BC drive in the OFF sublayer

The OFF sublayer of the IPL is not a pure OFF signal source; rather it contains significant numbers of ribbon outputs directly from the in-transit axons of ON cone BCs. In one sense this is not a new discovery. Non-mammalian bony vertebrates such as reptiles, avians, amphibians, teleost fishes all display multistratified bipolar cells and in fishes, ON bipolar cells have definitive synaptic outputs in the OFF sublayer (e.g. Sherry and Yazulla, 1993). In the past, bistratified mammalian BCs have been noted in Golgi preparations (e.g. Famiglietti, 1981), but the concept of dual ON/OFF signaling in the mammalian OFF sublayer appears not to have been seriously considered until ON BC axonal ribbons in the OFF sublayer were independently visualized at the optical level by Dumitrescu et al. (2009) and Hoshi et al. (2009).

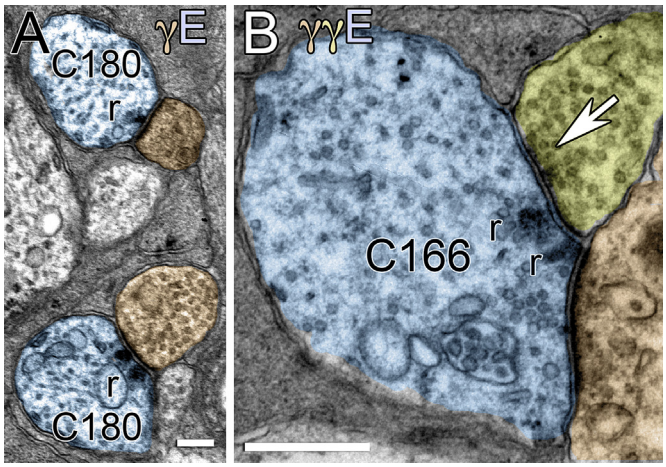

Fig. 5. Axonal ribbons in RC1. (A) Axonal ribbons (r) at mid-axon (blue) from CBb 180 (C180) to AC targets (orange) in the OFF sublayer. CBb 180 splits high in the OFF sublayer and makes axonal ribbons immediately after the split. (B) Axonal ribbons from CBb 166 (C166) onto two different targets (orange, yellow), one of which makes a feedback synapse (arrow). Note the distinctive postsynaptic densities in the targets. Scales, 500 nm. Recomposed from Anderson et al., (2011b) Molecular Vision by permission of the authors.

Connectomics has now validated these observations (Anderson et al., 2011b) both by showing presynaptic axonal ribbons and characterizing postsynaptic targets (Fig. 5). After mapping hundreds of BC axons, we showed that 36% of CBb cells form OFF layer axonal ribbons (Fig. 6), that the entire OFF layer contains axonal ribbon outputs from all CBb classes, targeting ON GCs that arborize in the OFF sublayer, e.g. intrinsically photosensitive GCs and bistratified diving GCs, as well as discrete sets of glycinergic ACs (GACs) and GABAergic ACs (γACs) for ON → OFF crossover (Lauritzen et al., 2012a). The diverse targets of axonal ribbons are summarized in Fig. 7. This an important concept in the generation of GC signal polarity, kinetics and temporal precision: multistratified cone BCs can multiplex signals in the ON and OFF sublayers (see below). This is an alternative to the notion that AC and GC stratification patterns alone control access to ON and OFF inputs. We have shown that monostratified ACs or GCs can be ON–OFF, that bistratified cells can be pure ON and that monostratified GCs in the OFF sublayer can be pure ON, similar to tyrosine hydroxylase (TH) immunoreactive axonal cells (AxCs). One may also ask why all CBbs do not show axonal ribbons. This issue is addressed in Section 3.8 *Sparse Networks and Joint Distribution Rules*.

But why might intrinsically photosensitive GCs and bistratified diving GCs arborize in the OFF layer to capture ON signals? Our connectomics mapping demonstrates that these cells also acquire direct input from OFF γACs, providing yet another ON motif initiated in the ON layer: cone > CBa > γAC > $_i$ ON GC, with a gain of n^2p. Since most inhibitory gains p are fractional (Wu, 1991), the direct ON (CBb) chain should have a higher sensitivity than the indirect ON (CBa > γAC) chain by a factor of p^{-1}. This suggests that multiple ON inputs might have different dynamic ranges and either extend response ranges or use different ON waveforms to shape total response functions, especially during light adaption.

3.3. OFF cone BC drive in the ON sublayer

The ON sublayer of the IPL is not a pure ON signal source; rather it contains significant numbers of ribbon outputs directly from fine

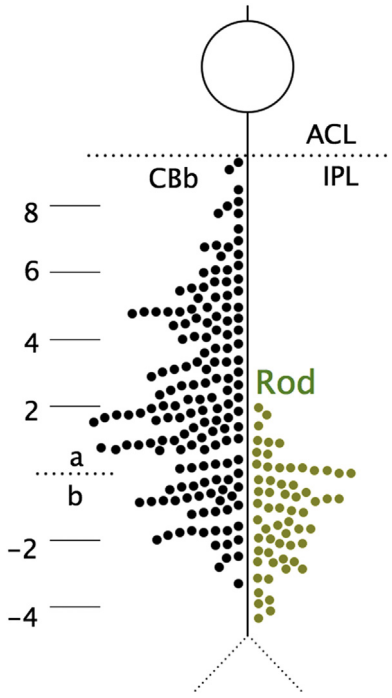

Fig. 6. Axonal ribbons. The distribution of 160 axonal ribbons in 54 CBb cells and 63 ribbons in 63 of 104 rod BCs in RC1. Ribbon positions are measured relative to the sublayer a/b border, defined as the proximal face of the nearest A_{II} AC lobule. CBb axonal ribbons are distributed throughout sublayer a. Rod BC axonal ribbons are excluded from 80% of sublayer a. Further, all rod BC ribbons exclusively target A_I or A_{II} ACs. From Lauritzen et al., (2012a,b) J Comp Neurology, by permission of the authors.

descending processes of OFF cone BCs (Lauritzen et al., 2012b). RC1 contains diffusely-stratified OFF cone BCs that synaptically target amacrine cells in the ON sublayer via fine descending processes. This architecture forms a large band of commingled ON and OFF BC inputs in IPL sublayers 3-5. These processes, often <100 nm in diameter, descend from the primary OFF sublayer into the upper part of the cone ON sublayer, mixing OFF CBa outputs in the same region as ON CBb cells. For example, intermixed ON CBb3 and OFF CBab2 terminal processes allow ACs to collect from both types to generate ON–OFF functions.

These new sets of BCs are referred to as CBab cells to indicate their dual outputs. But, importantly, they are canonical OFF cone BCs as they primarily arborize in the OFF sublayer, are coupled to other OFF BCs, are both presynaptic and postsynaptic to A_{II} AC lobules, and are glycine-negative. All these features are diagnostic of mammalian OFF BCs. The diversity of contacts is as complex as for axonal ribbons. Pushing the OFF inputs far past the nominal ON–OFF border and considering the complete mixture of CBb axonal ribbons in the OFF layer ultimately creates a central mixed ON–OFF band spanning about 75% of the IPL. The same ON–OFF excitatory drive is partitioned into GAC and γAC-mediated parallel channels that can target the same GC, which presumably shapes the response properties of the GC targets. CBab cells provide direct ribbon drive to at least one GC class in the ON layer. CBab cells also synapse on ACs throughout the nominal ON layer of the IPL, creating ON–OFF ACs that likely impact all CBb surrounds. These inhibitory motifs are both feedback and feedforward, targeting GACs and γACs, which in turn synapse onto CBa and CBb cells, and at least two classes of GCs. It seems that, by breaking the classical stratification rules of the IPL, CBab cells form specific ON–OFF subnetworks that could not otherwise be constructed. These unpredicted network topologies may underly widespread ON–OFF signals. Taken together, these new findings suggest a revision of the traditional view of IPL lamination in mammals to one more in line with the likely structure of non-mammalian retinas (Fig. 8). First, there is no pure OFF layer at all. Rather the OFF layer is "striped" with radial ON CBb axons that provide a sparse grid of ON inputs for specific neurons. Second, the great mid-zone of the IPL is populated by a block of ON and OFF cone BCs whose surrounds are explicitly

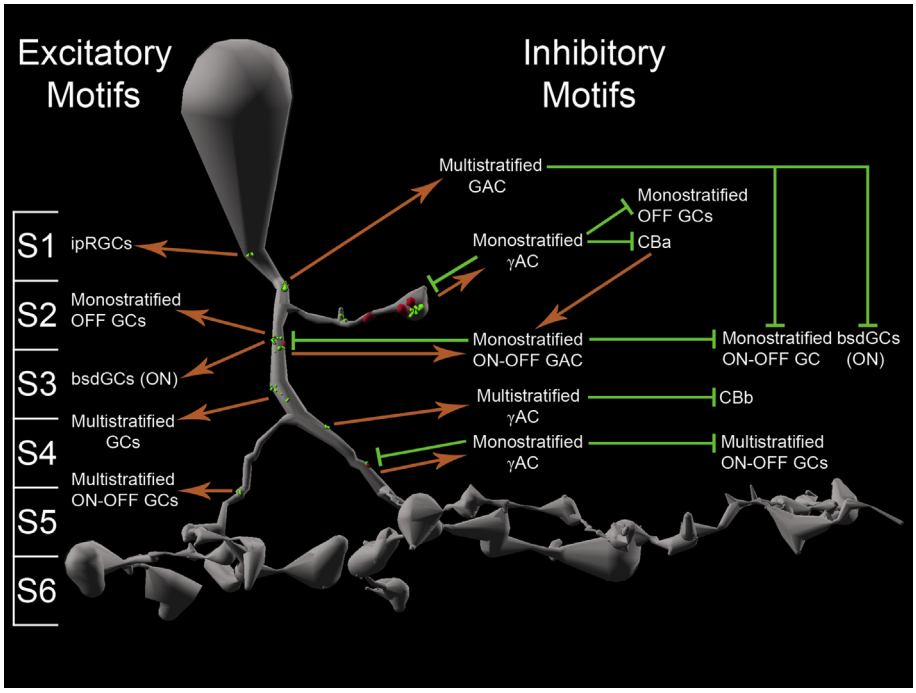

Fig. 7. A flow diagram for axonal ribbon motifs collapsed onto one canonical cell. Spatial distributions of axonal ribbons have been preserved to represent actual axonal ribbon locations. The axonal branch in sublamina 2 and the bifurcated descending axon are included for completeness, though both occur only in a minority of cone BC cells. In addition to abundant axonal ribbon output, CBb axons are frequently postsynaptic to ACs. S1-S6, IPL strata 1–6; red arrows, excitatory ribbon synapses; green flathead arrows, inhibitory GAC or γAC synapses; From Lauritzen et al., (2012a,b), J Comp Neurol, by permission of the authors.

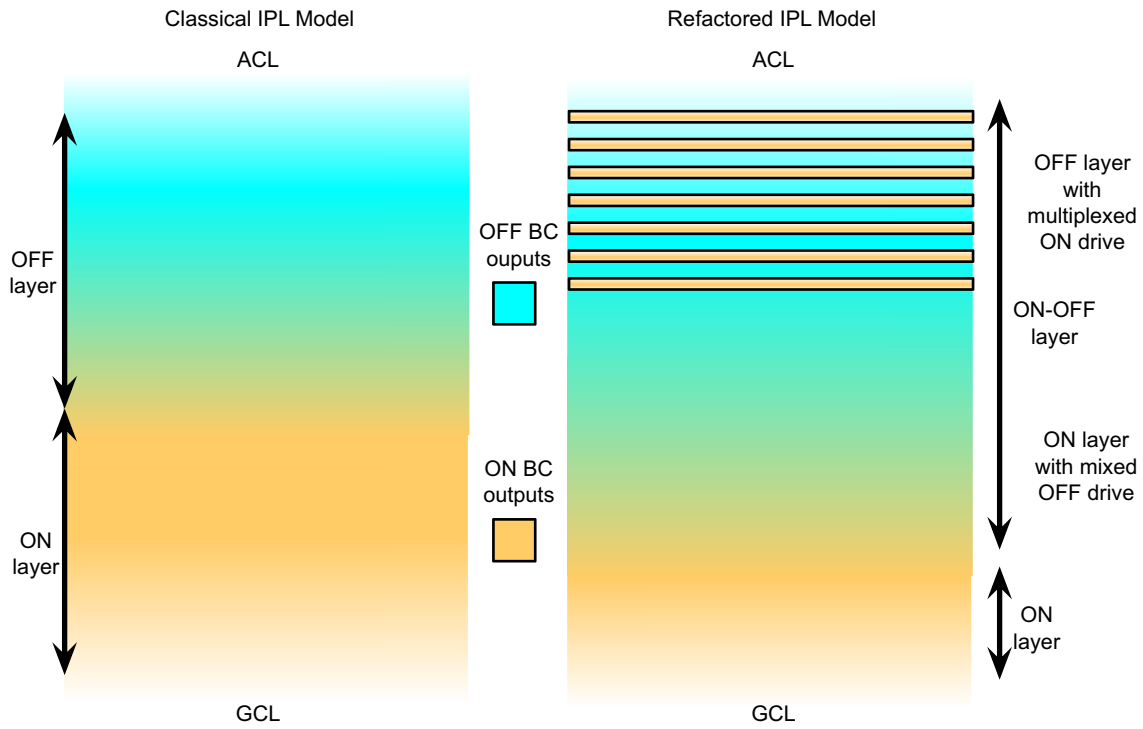

Fig. 8. The refactored IPL. The IPL begins at the ACL (top) and at the GCL (bottom). The density of ON and OFF BC outputs are represented in orange and cyan, respectively. The classical view is that there is some border between ON and OFF layers near mid-IPL (left). The refactored view (right) addresses the mixing of ON and OFF BC outputs (right). The strength of ON drive from CBb cells is distributed in discrete bands in the OFF layer and is continuously mixed in the ON layer. This creates an ON–OFF band that spans 75% of the IPL, leaving a thin pure ON band containing CBb cells and rod BCs.

ON–OFF by virtue of the dense mix of γACs and GACs that collect inputs from both ON CBb and OFF CBab cells and provide wide-field and narrow-field feedback respectively. Finally, the nominal "pure" ON zone is limited to a narrow band of rod BCs and mostly CBb6 and CBb wide-field cells. The critical feature of this new structure is that multistratified ACs and GCs can no longer be assumed to be ON–OFF, and that monostratified ACs and GCs can no longer assumed to be pure OFF or pure ON. Every cell's complete synaptic flow must be mapped, not inferred.

3.4. ON–OFF crossover motifs

A major network concept in retinal signaling is known as crossover: a net sign-conserving signal flow from ON → OFF and OFF → ON channels, dominated by GACs (Hsueh et al., 2008; Werblin, 2010, 2011). However, until the advent of connectomics, actually understanding nature and scope of crossover was literally impossible. The potential roles of crossover include compensating for synaptic rectification (Werblin, 2010), enhancing rectification (Liang and Freed, 2010) or improving contrast coding (Liang and Freed, 2012). The underlying schema for crossover is that diffusely stratified GACs transit the ON–OFF border to mediate, for example, CBb > GAC > $_i$ OFF GC chains where the GAC input provides an appropriate OFF polarity via an anionic current to compensate for AMPA receptor rectification. Of course, as we have shown, there is an extensive amount of ON–OFF signaling within the core of the IPL. We now know that CBb axonal ribbons provide an ON → OFF crossover topology to monostratified GACs in the OFF layer directly. Further, there are also CBb > γAC > $_i$ OFF GC chains in the OFF layer (Lauritzen et al., 2012a). So far, none of the CBb axonal output crossover elements engage A_{II} ACs in the nominal OFF layer. A_{II} ACs largely target CBa cells which means the net gain for the A_{II} > $_i$ CBa > OFF GC chain is np and likely rectifying. While there is extensive direct A_{II} synaptic drive to α and δ OFF GCs (viewed from the GC side), which are both strongly rectified GCs, the net gain will only be p, counterbalanced by even more extensive CBa2 input with gain of np. So GACs other than A_{II} ACs are likely the major source of rectification correction for the OFF layer. Those networks remain to be completely mapped but their presence is clear.

3.5. Rod-cone crossover suppression and winner-take-all networks

Psychophysics has long documented potent interactions between rod and cone vision, many of which are clearly winner-take-all in outcome (Brill, 1990; Buck, 2004; Frumkes and Eysteinsson, 1988; Goldberg et al., 1983; Lange et al., 1997; Stabell and Stabell, 1998, 2002; Thomas and Buck, 2006; Trezona, 1970, 1973), but the mechanisms have remained unknown. The idea that horizontal cells mediate such interactions (as in non-mammalians) has proved difficult to support and is complicated by the lack of evidence for axonal signaling in mammalian horizontal cells. Further, rod-cone interactions are fast, do not reflect the kinetics of horizontal cells and involve narrow fields inconsistent with horizontal cell coupling (Buck, 1997, 2004; Buck et al., 1984; Thomas and Buck, 2006). Finally, rods can induce a variety of chromatic effects (Stabell and Stabell, 1998). Connectomics provides definitive answers. At least eight unique suppression motifs between rod and cone BCs cells are mediated by several sets of ACs (Fig. 9). Cone suppression of rod signaling engages five different AC chains. All rod BCs are inhibited by CBb-driven ON γACs and GACs. A quarter to a third of AC synapses on rod BC terminals arise via ON cone ACs with a net cone → rod suppression of n^2p. All key elements of the rod BC pathway, including A_I and A_{II} ACs receive extensive cone-driven suppression. Each A_I AC is contacted by over 100 inhibitory synapses on its proximal dendrites in the OFF layer via CBa > γAC > $_i$ A_I AC chains and A_{II} ACs are targeted by cone BC > AC > A_{II} AC chains

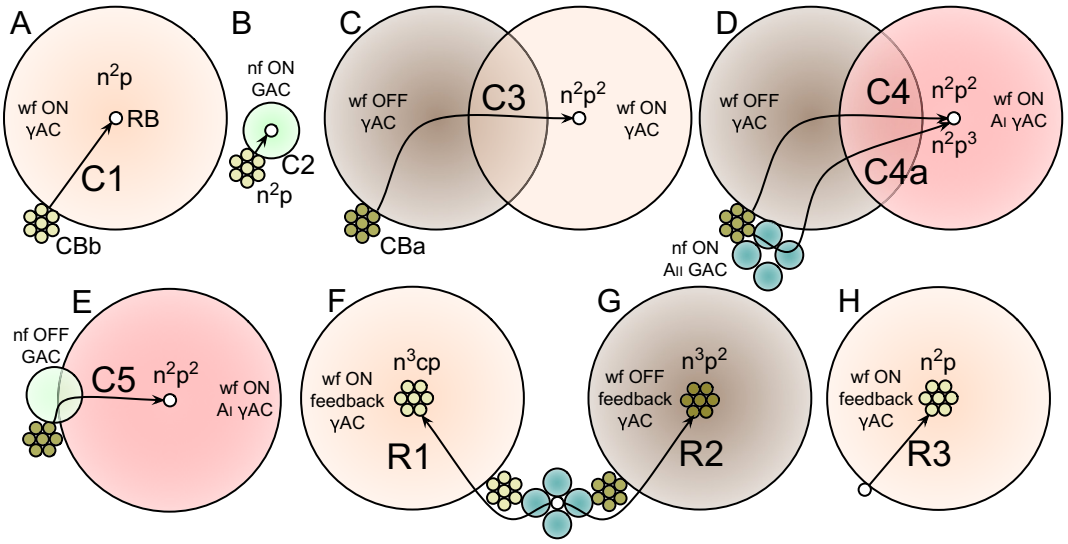

Fig. 9. Rod-cone crossover. Eight crossover motifs between rod BCs (white circles) and patches of cone BCs (honeycomb) mediated by fields of crossing AC processes (large circles). (A) Motif C1. Coupled CBb cells (tan honeycomb) are presynaptic to wide-field ON γACs that target single rod BCs (RB, white circle) in a chain synapses for a gain of n^2p (see Section 4.6). Each RB receives inhibition from a surrounding field of 15–30 CBb patches. Only three are diagrammed. (B) Motif C2. CBbs are presynaptic to narrow-field ON GACs that target single rod BCs. (C) Motif C3. CBa cells (gold honeycomb) are presynaptic to wf OFF γACs that target bistratified wf ON γACs in the OFF layer by somatic synapses, which in turn target rod BCs. (D) Motif C4/C4a. CBa cells are presynaptic to wf OFF γACs that target AI γACs in the OFF layer by GABAergic synapses on the proximal dendrites, which in turn target rod BCs. Some OFF γACs are also targeted by AII ACs in the chain. (E) Motif C5. CBa cells drive narrow-field GACs that synapse on the proximal dendrites of AI γACs. (F) Motif R1. Rod BCs drive AII ACs coupled to CBb cells. CBb cells are presynaptic to ON γACs that inhibit nearby and distant CBb cells. (G) Motif R2. Rod BCs drive AII ACs that are presynaptic to CBa cells, which drive OFF γACs to inhibit nearby and distant CBa cells. (H) Motif R3. Sparse rod BCs drive mixed rod-cone γACs that are presynaptic to large numbers of CBb cells. Lauritzen et al., in review.

throughout the IPL, including a highly selective inhibitory input from CBb > ON GACs that target rod BCs, A_{II} ACs and A_I ACs.

Rod suppression of cone signaling is driven by three motifs. Certain wide-field cone-driven ON γACs also collect sparse rod BC inputs and are both presynaptic and postsynaptic to CBb cells. In the scotopic–mesopic transition, this represents an RB > γAC $>_i$ CBb inhibitory chain with a gain of n^2p. However the most powerful motif is the full rod $>_m$ RB > A_{II} ACs:CBb > γAC > CBb chain with a suppressive gain of n^3p. Because A_{II} cells are narrow field elements (<100 μm) while the γACs are wide-field (>250 μm), each patch of rods can inhibit a vast field of surrounding cones.

3.6. Tiered cone bipolar cell coupling

In addition to the long-established A_{II} AC::A_{II} AC and A_{II} AC::cone BC coupling patterns first described by Kolb and Famiglietti (Famiglietti and Kolb, 1975; Kolb and Famiglietti, 1974a, 1974b), connectomics reveals extensive axonal coupling among cone BCs (Lauritzen et al., 2013). Coupling occurs within but not between CBa (OFF) and CBb (ON) superclasses. We find at least 13 distinct classes of cone bipolar cells: OFF CBa1, CBa1w, CBa1-2i, CBa2, CBa2w; CBab2; ON CBb3, CBb3-4i, CBb4w, CBb4-5i, CBb5w, CBb6w, and CBb7w (equivalent to previously identified wide-field cone BCs), where the number indicates a progressively more proximal stratification stratum, *i* denotes an interlaced axonal pattern bridging sheets of coupled bipolar cells, and w denotes wide field axonal arbors (>60 μm). CBb7w cells co-stratify with rod BCs. Coupling occurs within ON and OFF superclasses but not between ON and OFF. However, within each superclass, both in-class (e.g. CBb4w::CBb4w) coupling sheets and cross-class coupling tiers (e.g. CBb3::CBb3-4i::CBb4w) exist. Cross-class coupling occurs between neighboring CBb pairs because their stratifications overlap vertically and laterally. As most CBb cells appear to express Cx36 (Han and Massey, 2005), this may explain in-class and cross-class coupling.

So far, ON pathway tiered coupling bridges all sheets (≈10–19 bipolar cells/sheet in RC1) but completely excludes any CBa or rod BC. We propose that cone BCs use coupling to smooth signaling transitions across BC classes with different dynamic ranges. But since all CBb cells are also coupled to A_{II} ACs, it is unclear why CBb cells also engage in both in-class and cross-class coupling. CBa::CBa coupling is also extensive, and suggests that coupling may play a key role in setting up cone BC terminal tiling. Most CBb sheets clearly tile via tip-to-tip coupling (Fig. 10). Whether CBa cells also show cross-class tiering remains to be shown, but it is likely given the existence of bipolar cells bridging layers 1 and 2. The abundance of CBa::CBa gap junctions partly explains the many gap junctions in the OFF layer visualized by freeze-fracture (Kamasawa et al., 2006).

3.7. Heterocellular γAC::GC coupling

Dye coupling (e.g. Vaney, 2004; Vaney and Weiler, 2000; Xin and Bloomfield, 1997) and pattern recognition of small molecule signals (Marc and Jones, 2002) has clearly established the likelihood of gap junctions between ACs and GCs, but the identities of the source ACs, distributions of coupling sites and visualization of gap junctions has awaited connectomics. While details of the networks involved remain incomplete as of this writing, pieces are coming together quickly. First, the gap junctions between γACs and GCs are very sparse, small (often < 200 nm in extent) and are optically invisible amongst the vast numbers of gap junctions made by A_{II} ACs and cone BCs. A particular class of γACs, the ON interstitial AC (IAC), is exclusively a feedforward AC that collects from an extensive pool of CBb cells and is presynaptic to other γACs and selects GCs. Specifically it is coupled at several sites to GC 606, a large γ+ ON GC (Fig. 11). While GC 606 is alpha-like in somatic size, it differs in selecting from different classes of CBb cells across the proximal IPL. Given that ON alpha GCs are deemed not to be coupled to ACs (Hu and Bloomfield, 2003; Völgyi et al., 2013; Xin and Bloomfield, 1997), GC 606 is likely to be another class of large

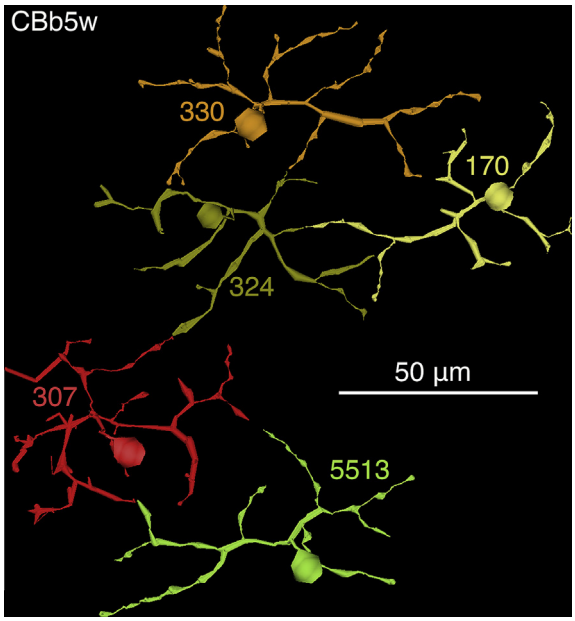

Fig. 10. Tip-to-tip BC coupling. A coupled tier of CBb5w ON BCs viewed in the XY plane (the retinal image plane). This is a new class of CBb cells that forms a precise stratum distal the new class of CBb6 cells and are coupled in-class via tip-to-tip junctions. Each cell ID allows tracking of all features in Viking (Lauritzen et al., 2013).

soma GC, but its physiology type remains unknown. GC 606 is also coupled to at least 5 different AC instances (separate cells) and likely more. The coupling signal into GC 606 arises from ON γACs in general and a cell (the IAC) which likely has a very strong ON response in particular. This sparse coupling is a further testament to the importance of ATEM connectomics. Such junctions are barely detectable with 2 nm resolution and impossible to find or validate with SEM based methods. Moreover, ATEM uniquely allows 0.3 nm resolution re-imaging to validate gap junction identities (Fig. 11D).

3.8. Sparse networks and joint distribution rules

The sites of signal transfer in the retina range from dense clusters of ribbon outputs by BCs to very sparse neurite sampling by ACs and GCs. The signal transfer functions between source cells A and target cells B is a joint distribution J_{AB}: the intersection between their individual neurite distributions: $J_{AB} = A_{xYZ} \cap B_{xYZ}$. These distributions formally include all forms of contact (e.g. adherens junctions, gap junction, presynaptic and postsynaptic junctions). Cell classes differ in neurite density and geometry (Reese, 2008), so the joint distribution will vary with pairing (Lauritzen et al., 2012a). As an example, GABAerigc γAC classes have large coverages with extensive overlap, while glycinergic GAC classes have modest overlaps. GCs largely tile with minimal overlap. It is mathematically impossible for all of these cells to interact uniformly, especially if their neurites are sparse. Different superclasses and classes have different Hausdorff dimensions, i.e. the amount of space-filling curvature they express in a plane. Hausdorff dimensions are very low for wide-field ACs and alpha GCs, and higher for BCs and directionally selective GCs. Put simply, it is impossible for every source and target to be optimized to achieve 100% contact. Since we don't know the sampling distributions for various cell classes, we must discover them by connectomics. Historically, the descriptions outflow of signals from one kind of cell to generic superclasses of targets (e.g. a given BC → ACs and GCs) has not been assessed in terms of joint distributions in a Hausdorff space, but this is an important future descriptor of networks. The important concept is that many signaling pairs, especially if their neurites are sparse, have a mismatch between the density profile of their output synapses A_{xYZ} and any cell's sampling of those outputs $A_{xYZ} \cap B_{xYZ}$ (Fig. 12).

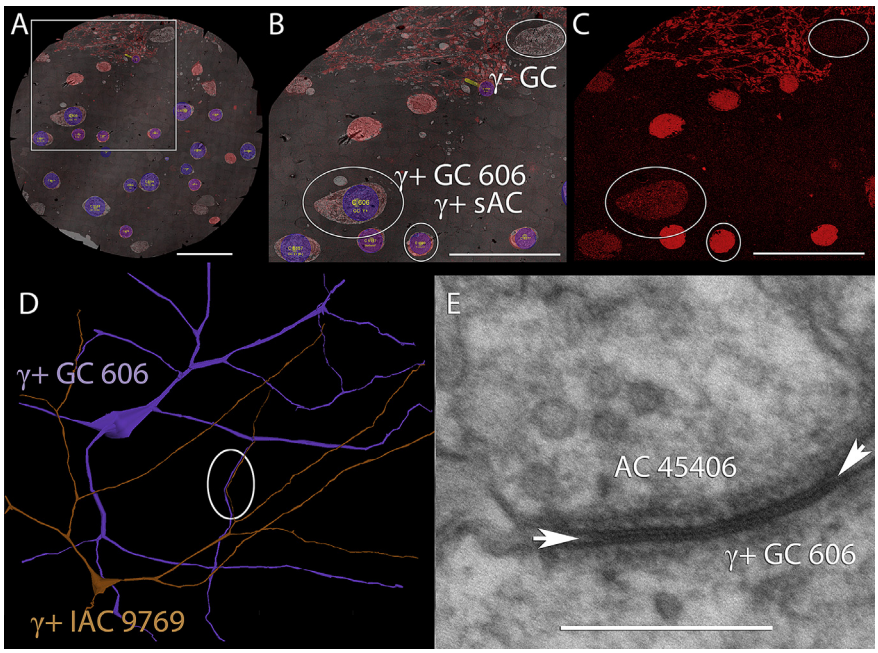

Fig. 11. GC::AC coupling. (A) Layer 371 of the RC1 dataset shown as a fusion of the GABA signal (red), the TEM imagery (greyscale) and the annotation overlay (blue). Scale 50 nm. (B) Scaled inset from panel A indicating three annotated cells with ellipses: a γ- GC, γ+ GC 606 and a γ+ starburst AC. Scale 50 nm. (C) The GABA channel from layer 371 showing the absence of any signal in the γ- GC, a moderate coupling signal in the γ+ GC 606 and a strong endogenous signal in the γ+ starburst AC. Scale 50 nm (D) γ+ GC 606 and γ+ IAC 9769 overlap and co-fasciculates at the ellipse. However coupling also occurs outside fasciculation sites. Panel width 243 µm. (E) Re-imaging of AC::GC coupling at 0.3 nm resolution. Gap junction between AC 45406 and γ+ GC 606 is slightly larger than 100 nm in extent (arrows). Scale, 100 nm. Sigulinsky et al., unpublished.

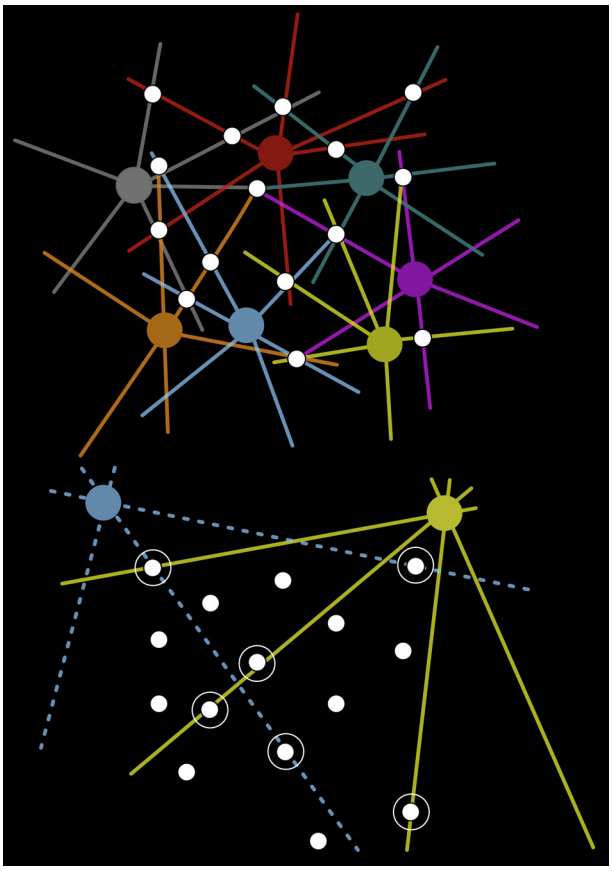

Fig. 12. How joint distributions influence sampling. A set of BC axons (white) traverses the retina normal to the image plane. (**A**) A high coverage cells are displayed as different colors for every instance. Each BC axon is contacted several times for an average contact of 2.4. In the bottom field, a two different classes of GCs (yellow, blue) form part of their tiling by overlapping dendrites and sampling from the BC grid. Most BCs are missed, for an average outflow contact of 0.375, which is meaningless. Six circled BCs are contacted by the GCs (none twice), and the GCs are errorless in contacting a BC that is encountered. The point is that GCs have low Hausdorff dimensions (they are not space filling) and their sampling is idempotent, i.e. further inputs would be superfluous. Modified from Marc et al. (2013), The New Visual Neurosciences, in press, by permission of the authors.

Concrete examples of joint distribution mismatch are (1) the axonal ribbons of CBb cells and their targets in the OFF layer (Lauritzen et al., 2012a), and (2) the outputs of A_{II} ACs onto the dendrites of GCs in the OFF layer (Anderson et al., 2011b). In both instances, sources far outnumber targets. A_{II} ACs have large Hausdorff dimensions and form far more output sites than are required to completely target all the GC dendrites in the OFF volume. However, OFF alpha GC dendrites traversing the OFF layer receive input from *every* A_{II} AC they encounter, with perfect efficiency. This means that the classical practice of measuring output percentages (e.g. percent output to ACs and GCs from a BC) and computing their variances has little meaning for network analysis.

In addition, we suggest that, rather than simply measuring the number of ACs targeted by a given BC, we should develop tools address an evolutionary, developmental and topological question: What connectivity achieves idempotent output for a specific network? Idempotency is the level at which additional inputs are superfluous for the function of a network selected by evolution. We are only now developing the genetic tools to test this hypothesis by targeting specific retinal cells and, ultimately, altering their synaptic sampling. Similarly, model bipolar cells for network analysis are only now being developed. But our mapping of cone BCs argues that they needn't all be proportionally contacted by wide-field ACs to achieve idempotent networks as they are embedded in a coupled sheet. Conversely, sampling the connectivity of a few BCs will never give a correct population profile of synapses for a network's motifs. Some retinal GCs and wide-field ACs sample relatively few excitatory synapses over 0.25 mm: ≈ 10 or so inputs per dendrite. This has two consequences: (1) noise reduction may be a major role of many feedback and coupling networks; (2) small fragments of ultrastructure may not capture true network design.

3.9. *Nested ACs: fine-tuning the retina*

It has long been known that serial AC → AC synapses are abundant throughout the IPL (Dowling, 1968; Dowling and Boycott, 1966; Witkovsky and Dowling, 1969). Indeed, AC synapses far outnumber ribbon synapses and the most common targets of most ACs are other ACs, the A_{II} AC being an exception as it predominantly, but not exclusively, signals CBa cells with glycinergic synapses and CBb cells with gap junctions. One hypothesis advanced by Dowling was that ACs were a mixture of inhibitory and excitatory neurons. On balance, all ACs appear to be primarily inhibitory (Marc et al., 1995), even if some have secondary excitatory neurotransmitters such as acetylcholine. So most serial synapses are likely concatenated inhibitions (Marc and Liu, 2000). One role of serial AC synapses is nested inhibition. For example, simple feedback inhibition can be summarized as a motif where a population of ACs is both presynaptic and postsynaptic to a population of BCs. In nested feedback, the ACs also inhibit each other. We previously showed that nested feedback and feedforward were common architectures in the fish retina and argue that they were analogous to nested

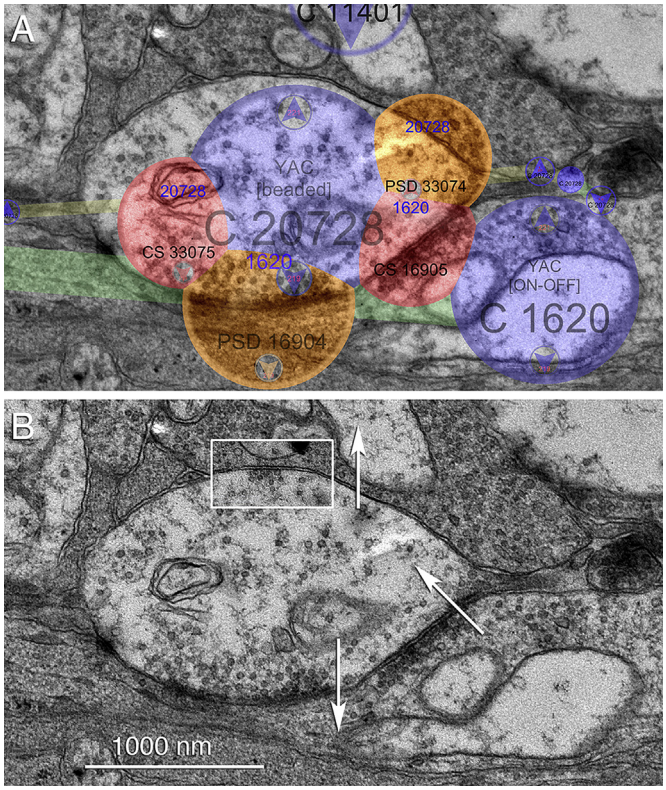

Fig. 13. Cross-channel synaptic nesting. (A) Viking annotation overlay in section 221 showing three cells, C20728 is a wide-field beaded ON γAC that receives input from CBb cells and is presynaptic to CBb cells, rod BCs (C 11401), other ON γACs (in class) and C1620, an ON–OFF γAC that receives input from both CBa and CBb cells. It is also presynaptic γAC 20728. (B) Annotations removed and an inset from section 224. Lauritzen et al., unpublished.

transconductance amplifiers (Xie et al., 1999) for tuning the temporal features of retinal networks and perhaps even configuring trigger features (Marc and Liu, 2000). Connectomics strongly supports this hypothesis by revealing the abundance of nested motifs.

Over 300 instances of cone pathway γACs have been traced in the rabbit connectome volume RC1 and they are all nested (Fig. 13), suggesting that simple feedback without nesting does not occur in any cone-driven network. Nested inhibition is likely a basic control motif for controlling the signaling dynamics of every photopic pathway. There are at least two modes of nesting (as with BC coupling): in-class and cross-class (Fig. 14). In-class nested γACs use feedback on the same class of γACs and a common class of BCs. Cross-class nested feedback γACs targets different cone BCs and or different γAC classes. A powerful example of cross-class nested feedback is rod-cone crossover, where different CBb classes drive wide-field γACs that target both rod BCs and other rod-cone crossover γACs. We don't yet have complete enough data to differentiate individual in-class and cross-class instances, but cases of both are abundant and some cells clearly dominate cross-class nested feedback (Marc et al., 2013).

The functions of nested feedback in general are not established, but three likely roles have emerged (Marc et al., 2012b; Marc and Liu, 2000). In the first, derived directly from control theory, nested feedback can be shown to suppress ringing in simple first-order feedback, thus increasing network bandwidth and fidelity. Second, depending on the strength of inhibitory signals, nested feedback may be critical timing elements of winner-take-all networks. Finally, crossover networks, largely but not exclusively driven by GACs, mediate signaling between all elements of ON and OFF channels. If we posit that ON → OFF crossover mediates rectification attenuation by delivering an anionic image of the ON signal (nominally an OFF signal), then both GCs and ACs in the recipient network should receive that signal to maintain network symmetry. Connectomics shows that to be likely based on network topology. Of course timing parameters will definitely have to be assessed by physiological profiling.

3.10. Towards a complete A_{II} AC profile

Profiling A_{II} ACs was an initial proof of principle for our connectomics initiative. If we could not rapidly replicate and extend the basic findings of the founders of retinal TEM imaging (Famiglietti and Kolb, 1975; Kolb and Famiglietti, 1974a; Strettoi et al., 1992), connectomics would need a critical reevaluation. As there are 39 A_{II} ACs in the retinal connectome RC1 (Anderson et al., 2011b), we have been able to data-mine the major attributes of A_{II} ACs, replicating all previous findings and significantly extending them (Fig. 15).

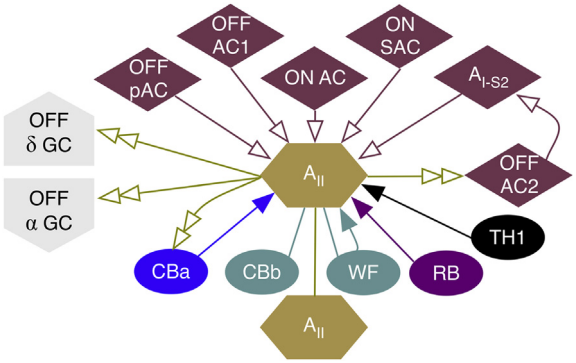

Fig. 15. The connectome for A_{II} ACs. There are four excitation paths (solid arrows), three coupling paths (lines), five modes of GABA inhibitory input (open arrows), and four inhibitory glycine outputs (double arrows). WF, wide field ON cone BCs; RB, rod BCs; TH1, class 1 dopaminergic axonal cells; α, alpha GCs; δ, delta GCs; pAC, peptidergic GABAergic AC; OFF AC1, dominant monostratified OFF cone AC population; OFF AC2, minor monostratified OFF cone AC population; ON AC, dominant monostratified ON cone AC population; ON SAC, ON starburst amacrine cell; AI-S2 subclass S2 class AI rod-dominated GABAergic AC. From Marc et al., (2012a,b) Current Opinion in Neurobiology, by permission of the authors.

The rod signaling pathway via rod BCs require A_{II} ACs as a critical low-gain fanout device to drive both CBa and CBb channels, but its direct engagement with photopic networks is also considerable. The precision of synaptic sampling (i.e. capturing a set of synapses within its arbor) by A_{II} ACs is much higher than the precision of cell sampling (i.e. capturing sets of cells within its arbor). A_{II} ACs in RC1 collect signals from $\approx 11 \pm 4$ BCs, the variability being determined by the intersection of the A_{II} AC and rod BC tileset. However, the coefficient of variation rod BC input is rather high (CV = 0.3). In contrast, each A_{II} AC captures $\approx$ 74 ± 5 ribbon synapses with a CV = 0.1. This is important from a developmental perspective, as variations in cell number across strains or individuals would appear to be readily normalized by the joint actions of coupling and synaptic sampling. In addition, A_{II} AC are 8-connected (7.6 ± 1) with neighboring A_{II} ACs via large gap junctions on their arboreal dendrites, further damping any variations in cell density on the local scale. A_{II} ACs drive all classes of cone BCs by either coupling to CBb cells or making glycinergic synapses on CBa cells. A_{II} AC lobules also drive OFF γACs that feedforward to A_I ACs in the OFF layer, and drive OFF α and δ GCs. Unlike cat retina, we have not yet found any evidence of output of OFF β-like cells. A_{II} ACs also receive a spectrum of inhibitory synapses, from both wide-field γAC and narrow field GACs, with at least six different class providing the drive.

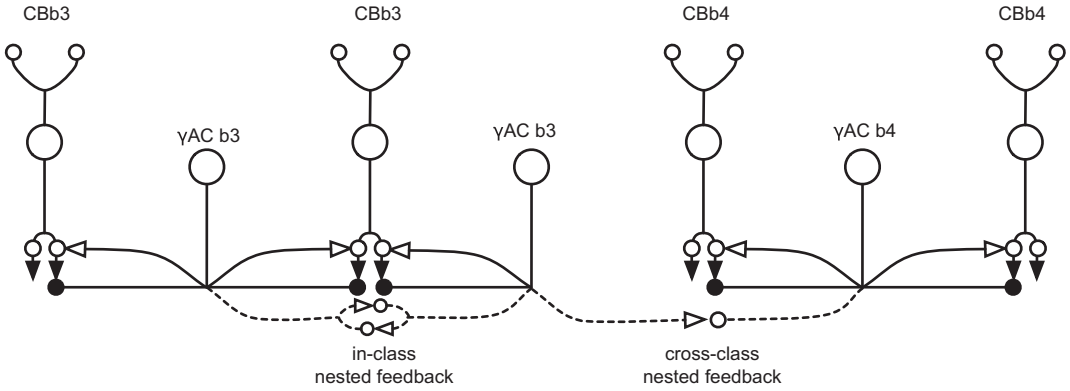

Fig. 14. In-class and cross-class nested feedback. Using CBb3 and CBb4 cells as examples, γACs selective for each class γAC b3 and γAC b4 can either target other ACs of the same (in-class) or different classes (cross-class). The feedback is nested because two AC engaged in BC feedback also inhibit each other.

The photopic excitatory drive of A_{II} ACs comes from four sources. Three are well known: (1) direct ribbon synapses from CBb cells, (2) direct ribbon synapses from CBa cells; and (3) extensive coupling to all classes of CBb cells (Famiglietti and Kolb, 1975; Strettoi et al., 1992). The fourth is new and somewhat controversial: somatic conventional synapses from glutamatergic TH1 axonal cells. The somatic synapses were first documented by Voigt and Wassle (1987). We demonstrated that rabbit TH1 cells distinctively display glutamatergic signatures (Fig. 16) in Anderson et al. (2011b). The ON responses of TH1 cells arise from CBb axonal ribbons (Dumitrescu et al., 2009; Hoshi et al., 2009) and likely drive A_{II} ACs by AMPA receptors. A_{II} ACs clearly have a complex set of drivers at every point in their scotopic and photopic ranges. Referring to the A_{II} AC as a "rod" AC makes little sense as over 90% of the connectivity of A_{II} ACs is cone-related, and it may be an archetypal cone pathway crossover cell.

3.11. New cell architectures

The characteristic ultrastructures of ribbon synapses, conventional synapses, gap junctions and adherens junctions have been known since the 1960s. Remarkably we have found several new contact architectures between neurons (Figs. 17 and 18). One of concepts emergent from modern proteomics is that every interactome has an architecture and specialized cell trafficking. Thus new contact features must reflect molecular relationships we have yet to associate with cytologic features in neurons. Traditional TEM photomicrography is a poor method for screening cell relationships. This is where connectomics is transformative, by automating imaging and data display and making connectomes open-access.

3.11.1. Cistern contacts

Cistern contacts (Figs. 17A and 18A) are typically (but not exclusively) made between ON cone BCs and their AC targets (Anderson et al., 2011b; Lauritzen et al., 2012a), often near axonal ribbons. They have a post-cisternal density that closely resembles a conventional postsynaptic density (PSD). The pre-cistern architecture is a single cistern of smooth endoplasmic reticulum (SER). We have no way to determine the polarity of the contact, but the similarity of the post-cistern to a classical PSD suggests the pre-cistern is a signal source. The SER-like cistern suggests further that lipid-based signaling may be involved and we propose that endocannabinoids could be produced or released there. Cannabinoid receptors are abundant in the inner plexiform layer (Yazulla, 2008) and appear to modulate the strength of inhibition (Middleton and Protti, 2011) but no architecture has been associated with endocannabinoid signaling.

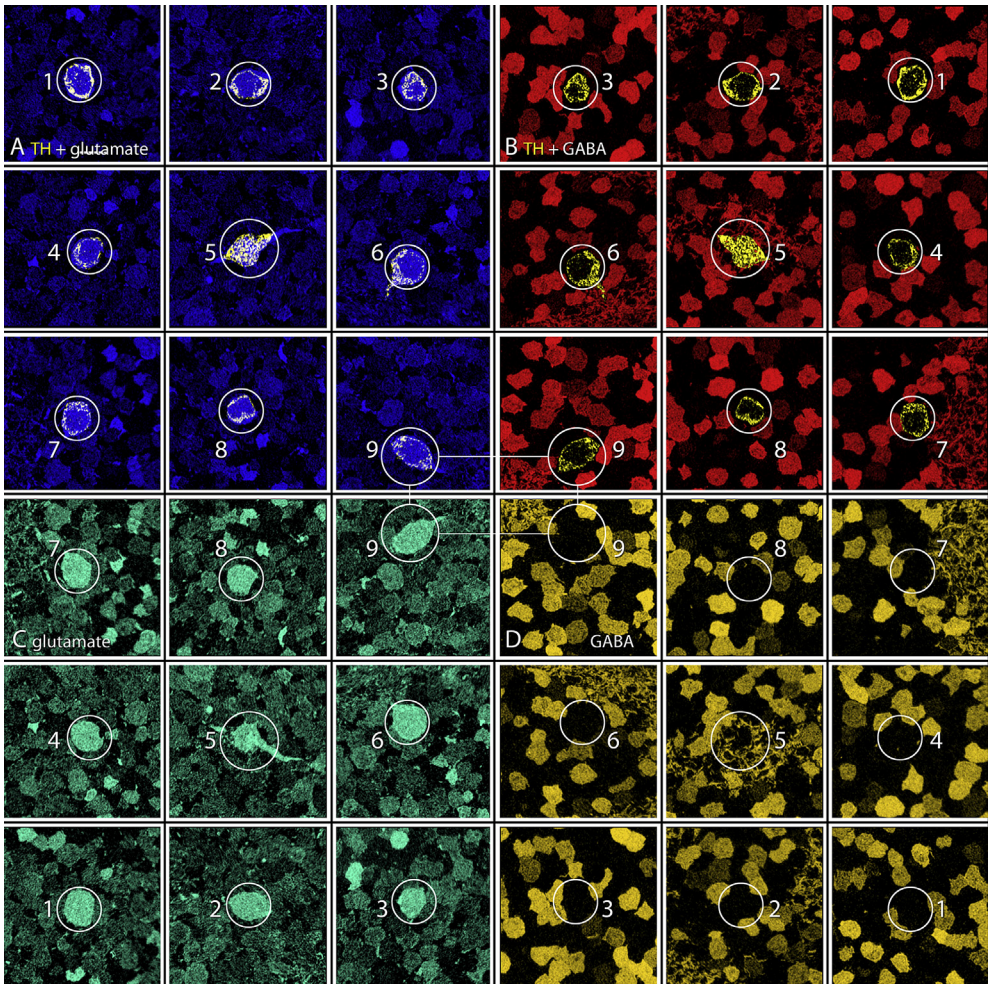

Fig. 16. Rabbit TH + cells have glutamatergic, not GABAergic signatures. Nine panels each showing one TH + cell from a single rabbit retina (A–I), probed for TH, glutamate and GABA in serial 200 nm sections. Each panel shows four mappings: upper left TH (yellow) + glutamate (blue), upper right TH (yellow) + GABA (red), lower left glutamate alone (cyan), lower right GABA alone (yellow). The location of each TH + cell is circled. Each TH + cell has a glutamate signal higher than the surrounding amacrine cell somas and equivalent to that of a ganglion cell. TH + cells have no measurable GABA signal. Scale, 10 μm. From Anderson et al. 2011b Molecular Vision, by permission of the authors.

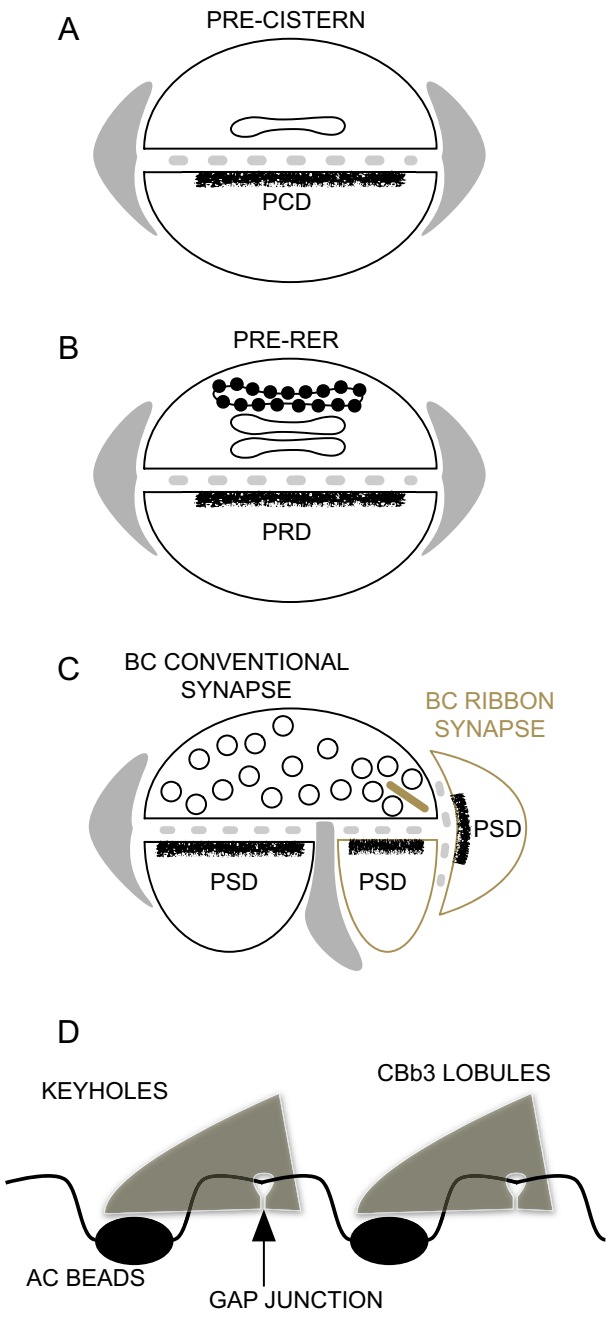

Fig. 17. New connection architectures. (A) Cistern contacts possess a single loop of SER in the pre-cistern element, a typical synaptic cleft of ≈20 nm with periodic densities in the cleft, and a post-cistern density (PCD) similar to classical PSDs. Typically, Müller cell processes (gray profiles) sheath BC axons and de-sheath to permit cistern contacts. (B) RER contacts possess 1-2 loops of SER capped by a ribosome studded loop of RER. The post-RER density (PRD) is similar to classical PSDs. (C) Conventional BC contacts are made exclusively by cone BCs onto processes with very large PSDs (black) usually adjacent to contacts involving synaptic ribbons and smaller PSDs (gold). (D) Keyholes are arrangements where a cone BC will form a self-gap junction at the edge of a terminal lobule around the connecting neurite of a beaded AC process. These neurites are typically 30–60 nm in diameter.

3.11.2. Rough endoplasmic reticulum (RER) contacts

RER contacts (Figs. 17B and 18B) form architectures very like cistern contacts. Though not as prevalent as cistern contacts, they are regularly found and are distinctive in possessing 2–3 flattened SER cisterns on the pre-RER side capped by a loop of RER, and a PSD similar to classical excitatory synapses. RER contacts can originate both in somas and processes, and we propose that they synthesize a signaling peptide whose nature prevents it from being trafficked rapidly, demanding local synthesis. There are many peptides whose distribution and modes of action remain unknown.

3.11.3. Bipolar cell conventional (BCC) synapses

BCC synapses (Figs. 17C and 18C) are large synapses that lack bipolar cell ribbons and are apposed to extremely large PSDs. Only cone BCs make these contacts and wide-field cone BCs make them with higher frequency than narrow field BCs. Additionally, nearby ribbon synapses form contacts with cells whose PSDs are typically less than 200 nm in extent while BCCs contact cells that make extremely large PSDs over 300 nm in diameter. It appears that CBa1w wide-field OFF BCs make few or no ribbons at all and exclusively use BCC contacts. While one might raise the question of whether this is really a BC, CBa1w has a bipolar form, a glutamate signal, AC targets and is postsynaptic to A_{II} ACs. Finally, BCC synapses target a subset of ACs and GCs and never appear to engage wide-field γACs. We propose that BCC synapses provide moderate gain transient outputs while ribbon synapses support sustained, high gain signaling.

3.11.4. Keyholes

Keyholes (Figs. 17D and 18D) are unique topological closures formed by certain cone BCs when a small axon terminal tendrils curl back and form a gap junction with the parent terminal in such a way that fine AC processes, as small as 30 nm, are captured in a tunnel of BC membrane. Whether this is epiphenomenal or a true attribute of cone BCs is not clear. The former is definitely possible as cone BCs are extensively coupled, probably through homotypic connexins, and there would appear to be no molecular mechanism to prevent self-linking. Alternatively these keyholes appear to repeat in neighboring BCs, are biased for cone BCs and selectively capture AC processes. We have not found any empty keyholes. Further, other cells that make homotypic gap junctions such as A_{II} ACs never form keyholes. If keyholes are functional, they may act as low-gain ephaptic signaling sites.

3.11.5. Microglia

Microglia (Fig. 19A,B) figure prominently retinal degenerations, but their fundamental roles in normal retina are uncertain. Surprisingly, microglia in normal retina showed large AGB signals suggesting responses to synaptic glutamate release. This could happen through at least three mechanisms: in vivo glutamate sensing by ionotropic glutamate receptors (e.g. AMPA receptors), purinergic channels, or stretch-sensitive channels in response to changes in intraocular pressure by injection. Microglia have been reported to express AMPA and NMDA receptors, metabotropic glutamate receptors, glutamate transporters, and display glutamate mediated chemotaxis (Guo et al., 2009; Liang et al., 2010; Pocock and Kettenmann, 2007). Our reconstructions of microglia show that they place small processes very close to bipolar cell synaptic ribbons without interposed Müller cells, suggesting they can directly sample glutamate release. While much research has focused on the tissue damage associated with microglial activation, their normal roles in retina are less clear. In CNS, microglia have been associated with regulation of synaptic plasticity (Wake et al., 2009, 2013), and some data suggest that normal glutamate activation of microglia leads to neuroprotective neurotrophin secretion (Liang et al., 2010).

3.11.6. Organized smooth endoplasmic reticulum (OSER)

Large-scale OSER architectures are uncommon but have been described in plants, fungi, and mammalian adrenocortical cells as a

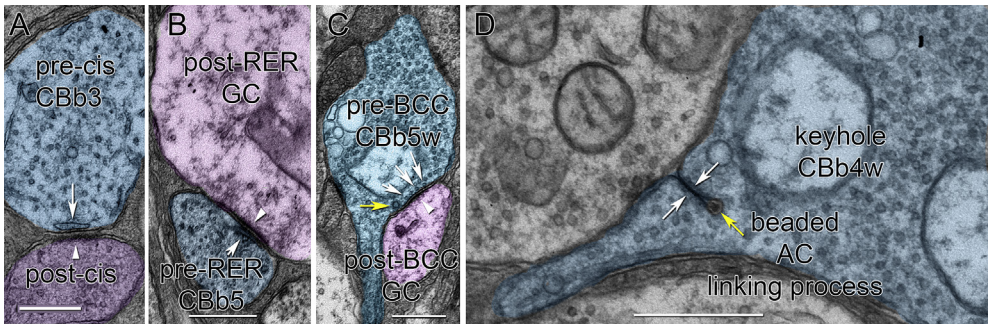

Fig. 18. ATEM imaging of new connection architectures. (A) Cistern contact between a CBb3 cone BC (blue, pre-cis) expressing a single loop of SER (arrow) and an AC (violet, post-cis) with a classic postsynaptic density (pointer). (B) RER contact between a CBb5 cone BC (blue, pre-RER) expressing a paired SER-RER apposition (arrow) apposed to a GC (violet, post-RER) with a classic postsynaptic density (pointer). (C) Conventional contacts between a CBb5w cone BC (blue, pre-BCC) with vesicles directly attached to the presynaptic membrane (white arrows) and a coated endocytotic omega figure (yellow arrow) apposed to a GC with a classic postsynaptic density and cleft (pointer). (D) A keyholes formed by a CBb4w cone BC (blue) via self-gap junctions (paired white arrows), trapping a linking process of 30 nm diameter from a beaded AC. All scale bars are 500 nm. Fig. 19A is from Anderson et al. (2011a,b), by permission of the authors.

possible specialization for lipid metabolism, and in other mammalian cell types (Korkhov and Zuber, 2009; Snapp et al., 2003). The retinal connectome reveals that rabbit retinal Müller cells form OSER-like aggregates: triangular SER meshes aggregate into large 5–9 μm diameter organelles located in their end feet (Fig. 19C,D). If these glial OSER aggregates function like smooth muscle SER in calcium transport, they may represent a massive calcium buffer for retinal signaling.

3.12. Summary of new connectomics discoveries

In summary, connectomics demonstrates that mining the full connectivity of any cell is not just a simple validation of older network concepts. All networks are proving to be far more complex than anticipated. There are at least nine major areas in which new motifs or functions have been disclosed.

- *Connectomics refactoring of the IPL* reveals that photopic CBb drive spans the entire IPL (not just the distal half) and photopic CBa drive penetrates deeply into the ON layer. The central core of the IPL is composed of an extensive ON–OFF subnetwork and ON–OFF signals likely pervade most GC outputs. This refactoring also demonstrates that bistratified cells can be ON and that monostratified cells can be ON–OFF. Thus, stratification does not predict response pattern: connectivity does.
- *Rod-cone crossover suppression* is deeply embedded in all IPL networks. Every CBb and CBa can drive rod BC inhibition and every rod BC can drive CBa and CBb inhibition via a vast web of ACs. The eight distinct pathways for rod-cone suppression are likely the complete rod-cone interaction architecture.
- *ON–OFF crossover inhibition* driven strongly but not exclusively by GACs is realized in multiple ways. Narrow-field multi-stratified GACs clear mediate some crossover, but much of it is also delivered via CBb axonal ribbons and CBab descending processes.
- *Tiered cone BC* coupling was completely unexpected but is pervasive. As most CBb::CBb and CBa::CBa coupling instances involve gap junctions smaller than 200 nm, they will be undetectable by optical microscopy. All CBb and CBa cells are coupled within their respective superclasses (e.g. CBb::CBb). However in-superclass coupling is tiered as it includes dense in-class (e.g. CBb3::CBb3) and cross-class coupling (CBb3::CBb4::CBb5::CBb5w). This means that there are several signaling paths through the cone BC network to GCs. Understanding the scope

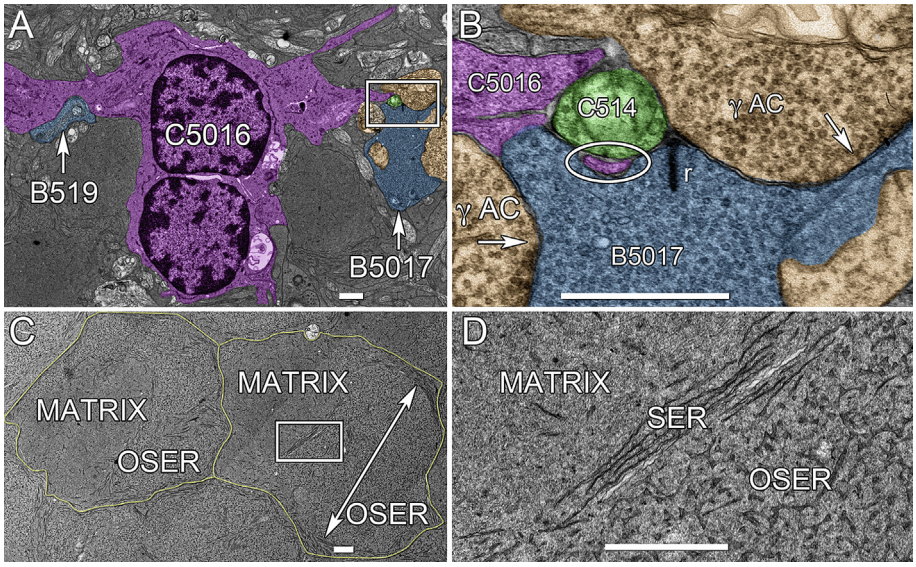

Fig. 19. Novel roles for non-neuronal cells. (A) A binucleate microglial cell C5016)with lateral processes contacting rod bipolar cells B519 and B5017. (B) The inset from panel D showing Insertion of a microglial process (oval) close to the synaptic ribbon (r) of rod bipolar cell B5017. (C) A section through the endfeet of two Müller cells (outlined) at the retina-vitreous border. The endfeet contain a filament-rich matrix and a large organelle of OSER. Arrow, 9 μm. (D) The inset from panel C showing the transition between the core matrix and the OSER organelle, bounded by SER stacks. D-G Scales, 1000 nm. Marc et al., unpublished.

of signal sharing across GCs via tiered cone BCs coupling will require new physiological and modeling endeavors.

- *Sparse heterocellular coupling* is yet another mechanism for signal propagation across retinal subnetworks. Specific γACs engage in coupling with GCs. Taken together with tiered BC coupling and extensive drive of all classes of cone BCs by A_{II} ACs, there are multiple non-synaptic paths between BCs and GCs. While the purposes of these coupling networks are not clear, combined with refactoring of the IPL, they could definitely participate in image coding by setting first-spike latency signals as proposed by Gollisch and Meister (2008), or the global projective fields of certain ACs described by DeVries et al. (2011). Recent findings in rabbit and mouse suggest that GC coupling mediates spike correlation (Hu and Bloomfield, 2003; Völgyi et al., 2013).
- *A_{II} ACs* are clearly deeply embedded in photopic networks. While previous models presented them as very simple rod pathway cells, they make at least sixteen different kinds of contacts making them by far the most complex neuron known. Further, they have five distinct sign conserving inputs spanning the entire visual dynamic range. How the diverse inhibitory inputs shape their response properties remains to be resolved.
- *Sparse networks* where a given cell makes only one or two connections with a given target are likely the norm in retina. Most of the AC inputs to BCs arise from single instances of a cell, and similarly BC outputs onto most cells involve one or two ribbons in transit. For example, a wide field AC that targets a few BCs in a 250 μm span may receive only a single BC ribbon input, suggesting that single or a few excitatory conductance events may control entire dendrites in some cells.
- *Joint distribution rules* accommodate the simple fact that different Hausdorff dimensions for cells at both the neurite and connection level make it impossible for all cell types to uniformly provision all targets or sample all sources. Thus it is critical to attend to the statistics of target rather than just source architectures.
- *Nested AC networks* are the most common synaptic architecture in the retina but no definitive role has been proven for them by physiological methods, in part because it has not been possible to target known nested partners. However, it is clear that most mammalian cone γACs engage in both in-class and cross-class nesting (e.g. motif C1 rod-cone crossover ACs), so modeling similar to that in goldfish (Marc and Liu, 2000) is likely to be appropriate for mammals.
- *Novel connection architectures* suggest that a significant amount of neuronal cell biology has been heretofore invisible. What the different appositions mean will clearly require molecular exploration in combination with connectomics. Nevertheless, there are many signaling processes such as cannabinoid signaling whose sources and targets have not been characterized. Our new contact morphologies could clearly be involved. In addition, it is likely that cone BCs can signal from conventional ribbon-free sites and we proposed this enables them to function simultaneously as sustained and transient cells.

3.13. Future directions for connectomics

Completeness is a new goal in neuroanatomy. Graph enumeration formally proves that the structural complexity of any large scale network transcends every inverse analysis every devised. Deciphering the correct topologies of retinal and brain network are NP-complete problems which no modeling or physiological approach can ever untangle. Deciphering the individual motifs of retinal networks requires the discovery all cell classes and mapping all their contacts and contact patterns across multiple instances of each class. The very fact that every network we have explored has exposed new, previously unknown connection motifs (Anderson et al., 2011b; Lauritzen et al., 2012a; Marc et al., 2012a) validates this view.

Measures of completeness in any analysis depends on the matrix we choose to fill for a topology mapping. Adjacency matrices require discovery of all partners in networks. Weight matrices require quantification of the numbers, locations and sizes of all contacts. Even within a connectome, defining completeness can be a challenge. Arguably, the variance of some measure should be asymptotically minimized when sampling approaches completeness. However we are still discovering those what those metrics should be. Classical measures may turn out to be useless or even misleading in defining completeness. Viking annotation allow automated tracking of variances on every synaptic feature (neurite diameters, intervaricosity distances, presynaptic vesicle cloud size, ribbon size, postsynaptic density size) within classes, superclasses and any other grouping. A major finding, in our view, is the demonstration that synapse number collected by a given cell type has an extremely small CV compared to other measures, implying that neurons can regulate synapse number even though cells may have quite variable dendritic or axonal overlap geometries. Further, there are spatial variances that have no meaning for characterizing network topologies, such as the percent of *output* from a given cell: partitioning of output is not a functional metric since there is no topologic or physiologic basis for presynaptic loading patterns influencing any single individual output. In contrast, how any spatially complex or sparse postsynaptic cell class samples the grid of an output class as the input to a spatially complex cell is absolutely central to understanding the development and function of networks. Completeness can also be assessed by edge density in network graphs where submotifs can be extracted and quantitatively compared.

There are several basic issues that must be addressed in assessing whether an approach or technology is capable of achieving complete network specifications. First and most importantly, spatial resolution limits the size of practical volumes. We know that a resolution of at least 2.2 nm is necessary to achieve errorless and complete annotation of all synapses and gap junctions. Further, that resolution has also allowed discovery of new cell relations (e.g.Lauritzen et al., 2012a). A recent review of connectomics inexplicably touted a resolution of 10 nm as adequate, which is clearly incorrect (Kleinfeld et al., 2011). If we accept the idea that mapping spine architectures, SER disposition, synapse sizes, and gap junction distributions are important (Bourne and Harris, 2011; Kamasawa et al., 2006; Massey, 2008), TEM remains the gold-standard. And TEM resolution also sets the standard for quality and completeness of synaptic identification, measured against a real ground truth. Our data suggest that statistically based autodetection schemes are not yet functional, and the parameters on which such a scheme might be based are still debatable. Our data on synapse versus incidental contact identification are exactly opposite those published by Helmstaedter et al. (2013). While ours are validated by high resolution reimaging ground truth, those of SBFSEM cannot be.

Second, it is not practical to rely on connectomics alone to segment cells. The same complexity that challenges inverse solutions also requires nearly complete mapping before classification can be attempted based solely on network features. Molecular tools are far superior for classification, as described below, and TEM is a superior platform for embedding molecular tags. Independent determinants of identity such as molecular (Shu et al., 2011) or optical (Bock et al. 2011; Briggman et al., 2011) tagging to segment populations can pre-validate classes and pre-select specific network elements for annotations. This is especially useful for developing

statistical profiles of cell classes and readily steers hypothesis-guided analyses in connectomics.

Third, we propose that shared networks of ATEM platforms are essential for synaptic connectomics (Anderson et al., 2009). While it is also possible to build specialized tools for connectomics, the scientific community needs general-purpose high resolution commercial systems far more than limited resolution platforms. ATEM systems also have a significant future role to play in the evolution of a histomics, the analysis of cellular arrays in all tissues. Our next objective is to develop statistically robust mini-connectome approaches, largely steered by CMP, to study the evolution and development of retinal networks, and pathoconnectomics technologies to explore neurodegenerations (Jones et al., 2011, 2003).

4. Definitions and advanced topics

4.1. Connectomics definitions

Connectome: The complete set of cellular partners and connections for a neural region. Connectomics can be executed on the mesoscale (spatial resolution of magnetic resonance imaging or even conventional optical imaging) to map fiber networks, or on the nanoscale (spatial resolution of electron imaging) to map synaptic networks.

Canonical Field: In a large scale network of repeating motifs, a canonical field (area or volume) contains a selected number of repeats, e.g. one copy of the rarest cell or *n* copies of central cell in a dominant pathway. Defining a canonical field requires domain knowledge.

Coverage: The amount of a given plane or volume that an object's tile or convex hull covers in 2D or 3D space. There are three kinds of coverages in tiling geometry: packings, tilings and coverings. A set of non-overlapping cells spread over a plane, e.g. blue cones, is a *packing* and with a coverage of <1. An exact coverage of 1 is a *tiling*. An overlapping coverage >1 is a *covering*. Cells such as ganglion cells approximate tilings, while most amacrine cells represent coverings. These assessments are based on modeling of a cell's possible field of interactions as a topological disk, specifically a convex hull of its dendrites or a parametric ellipsoidal disk superimposed on this field. The nominal coverage C for a cell with a planar density of D cells/unit area and a convex hull area of A units/cell is D*A.

Hausdorff dimension: A measure of the space-filling capacity of a structure, e.g. a collection of neuronal dendrites. The Hausdorff dimension is a general descriptor of non-integer dimensions, related to fractal or box-counting Minkowski dimensions. The notion is that a dendritic field can be viewed as a collection of 1-dimensional lines traversing a 2-dimensional area. Thus the Hausdorff dimension is a non-integer value that specifies how closely the dendritic field approaches a higher dimension, i.e. how much area is traversed.

Interactome: The complete set of molecular partners and pathways for a defined cell class. It usually refers to an interacting sets of proteins, small molecules and ions, and is often expressed as an undirected graph for simplicity. A key to network theory is that graphs of different biological domains (cell topology, electrical signals, molecular signals) can be nested in matrices to create rich mathematical models.

Joint distribution: Formally, the intersection of one or more n-variate distributions. For connectomics, we consider a joint distribution as the physical intersection probability of neurites from different cells. This is the outcome of both coverage and Hausdorff dimension: how many contacts are possible between a given pair of cells. As an example, consider signaling from sets of source cells A and target cells B, where their neurite patterns in the IPL are described by volume distributions A_{xYZ} and B_{xYZ}. Their interaction space is a joint distribution J_{AB}, the intersection between source and target neurite distributions: $J_{AB} = A_{xYZ} \cap B_{xYZ}$.

Nested networks: In any network architecture, there are two kinds of nesting: hierarchical and simple. Hierarchical nesting means containing another entire network within a node or vertex. Simple nesting involves reentrant signal loops in a network. Marc and Liu (2002) introduced the term to refer to different kinds of feedback and feedforward loops in retina with reentrant features. The concept was originally introduced as *nested transconductance* in the design of high-fidelity, low-power solid state audio amplifiers (e.g. Xie et al., 1999).

4.2. Graph theory definitions

Graph Theory: The study of networks and, ultimately, the analysis of connection patterns and how signals travel through networks. Importantly, many formal theorems about networks and their underlying motifs (stereotyped components) scale to massive levels. Graph theory thus lends itself to the analysis of large biological networks. There are several excellent textbooks on graph theory and we highly recommend Bollobás (1998) and Diestel (2010). The latter, in particular, has a rapid electronic updating schema keeping the interested reader abreast of new findings.

Network Graph: A graph G(*V,E*) is a set of connections or edges (E) among discrete elements called vertices (V). Distinct edges between vertices can be *undirected (bidirectional)* or *directed* and the constructed networks can be thus undirected, directed or mixed. Biological neural networks are generally mixed due to the inclusion of both directed (chemical synapses) and undirected connections (gap junctions). Moreover, more sophisticated graphs can include asymmetrically bidirectional connections. For those familiar with electrical circuits, many critical aspects of network graph theory were developed by Kirchoff. Unlike classical lumped-parameter representations of current flow, network graphs are general descriptors of processing that can include complex topologies, biological specificity, distributed and compartmental features, and even non-stationary features in matrix representations (see below). A simple graph allows only a single edge between vertices and no loops. Graphs that represent real biological networks permit multiple edges and loops. Visualizing networks with multiple edges requires weighting rules to *aggregate* or combine multiple edges.

Adjacency Matrix: A connectivity matrix of the number of edges E_{ij} between every vertex pair *i* and *j* in a network of *n* vertices. All connections have $E_{ij} \neq 0$. All non-connections have $E_{ij} = 0$.

Weight Matrix: A connectivity matrix representing the edge weight or strength (in defined units) between every vertex pair in a network.

Connections and Non-connections: See *Adjacency Matrix* above. The occurrence of an edge or connection between a pair of vertices or cells is a nominal proof of its existence, and its expected density can be computed from spatial dimensions of the chosen canonical field. Evidence of a non-connection, however, is statistical, as one can only assert the absence of a connection over a sampled field, compared to realized connections. There are two types of non-connections: those arising from lack of opportunity (spatial separation were two kinds of cells never touch) and those arising from rejected connections *despite* opportunity (e.g. cells touch but never synapse). The latter implies deterministic processes in network assembly.

4.3. Classification theory definitions

Classification: Assigning an observation (a data vector of dimension N) to a class (category) based on partitioning of the

entire N-space. Conceptually, classes are hypervolumes defined by N-space centroids and their statistical moments. Analysis of a large collection if data vectors by clustering algorithms partitions the N-space and defines the class centroids. (Marc et al., 1995) provide a description of typical clustering for unsupervised classification (see below). An excellent text on classification is Duda et al. (2001).

Supervised and Unsupervised Classification: There are two types of classification. Supervised classification employs user-selected *signatures* (N-space centroids) derived from previously acquired ground-truth data to determine the classes into which new observations will be placed. Predetermined signatures are "supervisory." Unsupervised classification computes class numbers, centroid and decision boundaries from a collection of data vectors. Signatures are computed from derived classes in an unsupervised mode.

Computational molecular phenotyping: A method of phenotyping cells using quantitative multichannel molecular imaging, measured molecule concentrations as data vectors, and unsupervised classification of the molecular N-space. The expression was introduced by Marc and Jones, in 2002.

4.4. Graph theory and connectomics

Graph theory (Bollobás, 1998; Diestel, 2010) is the formalization of how we discover, describe, and analyze networks of all types, including retina. The idea that the retina is a simplified part of the brain is supported by neither molecular biology, connectomics nor graph theory. Indeed, the vertebrate retina may represent the most complex packing of functional networks that has ever evolved: no brain region has as many identified different kinds of neurons or synaptic networks per unit volume. In graph theory, cells that integrate signals from other cells are termed *vertices* (V) and the connections they form via synapses, gap junction or other spatially discrete signaling modalities are nominally termed *edges* (E). Any set of connected vertices (a,b,c) can be described as a collection of edges (e.g. ab, bc), a path (abc) or a circuit (abca).

Any graph G can be defined by a matrix of vertices and associated edges (V, E). Vertices are connected by undirected edges or directed edges (arcs) and we assume that gap junctions and chemical synapses are their underlying biological forms. Graphs may be undirected (all bidirectional edges), directed (all unidirectional edges), or mixed; the latter is the norm for biological neural networks. For simplicity we will consider all connections as edges and track their directionalities parametrically (Fig. 20). In a simple graph a single vertex may contact another vertex by a single edge, but in biological systems our graphs must permit multi-edge connections. After rules are established for aggregating multiple edges, we may be permitted to collapse multiple edges to single weighted edges.

There are degrees of completeness in describing networks. Formally, a connectome is the *adjacency matrix* for a collection of neurons in a canonical region that includes all partners and definitive non-partners. A subtle point is that the tabulation of all non-connections is as important as the tabulation of connections and demands the same robustness of analysis. Defining non-connections can be achieved by connectomics but not by routine anatomy. A functionally complete network graph is a *weight matrix* tabulating individual transfer functions (e.g. synaptic gains, polarities, kinetics, etc., perhaps aggregated as a global transfer function) for all vertices. We ultimately seek the latter, as well as the rules for combining edges at a vertex. Connectomics can ultimately provide critical information for discovering the true network topology of a system and the framework for estimating its weights.

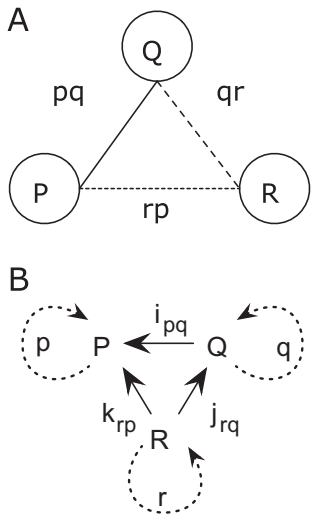

Fig. 20. Simple network graphs. (A) An undirected graph with vertices PQR and bidirectional edges pq, qr, rp. (B) A complex direct graph with vertices PQR, directed edges i (p → q), j (r → q), k (r → p), and re-entrant edges pqr.

How might this be done with connectomics? For example, weighting connections partly includes knowing the numbers, spatial locations, sizes and molecular classes of synapses and gap junctions, which connectomics can provide. While present techniques are not fully compatible with antibodies for marking known molecular classes of synaptic receptors and connexins, that is under aggressive development (Micheva and Bruchez, 2011; Micheva et al., 2010; Micheva and Smith, 2007). And while physiology is essential for determining the polarities and kinetics of identified synapses under various states, those data can only be used in a network model when we know how many such synapses are distributed over a target cell. Locations of synapses are unimportant if a cell is provably electrotonically compact, but compactness cannot be assumed. Thus the locations of synapses are a rich new source of data for modeling. Finally, physiology can estimate total currents driven by some synapses but there are no instances where physiology has been able to achieve this for every synapse on a cell. Mammalian cone bipolar cells receive up to 100 individual synapses from nearly as many individual amacrine cells drawn from at least five different classes. Some ganglion cells receive over 1000 synapses of different postsynaptic morphologies and sizes, each of which can be specified by connectomics, but not by physiology. Every type of synapse has a distinct average postsynaptic density size and vesicle cloud of a discrete number of vesicles. Knowing the likely unitary conductances and sizes of distinct receptor and connexon subunits and the size of the assembly should permit very robust weighting. Physiology is essential for broad characterization of function, but lacks the granularity of connectomics.

The first major contribution made by graph theory is a concrete definition of network diversity. Graph enumeration theory describes the possible network architectures of a given system (Harary and Palmer, 1973). Some important relations expose how quickly network diversity can overwhelm inference. The number of undirected (U) networks possible with n vertices is:

$$U(n) = 2^{n(n-1)/2} \tag{1}$$

Adding directed (D) connections admits increased network numbers:

$$\mathrm{D}(n) = 2^{n(n-1)} \tag{2}$$

Even a simple undirected graph made from three vertices (e.g. P,Q,R) can be connected 8 unique ways via the edges p,q and r:

none, p, q, r, pq, qr, rp, pqr (Fig. 1A). A mixed directed and undirected graph of the same 3 vertices admits 64 unique versions. In the vertebrate retina, with ≈70 cell classes (Marc, 2010), $D(n) = 9 \times 10^{1473}$. For brain, where we estimate that over 1000 classes of neurons exist, based on known neuronal diversity and the over 250 brain regions estimated from cortical parcellations (Van Essen et al., 2011), $D(n) = 1 \times 10^{300728}$. These massive numbers beggar the ability of even the fastest computers to sort and model them. Such subgraph isomorphism problems are NP-complete (Karp, 1972).

But are all of these theoretical networks useful? Is there no way to prune them down to a useful set? Unfortunately, there is no ready shortcut, as a *gedanken* experiment will show. Imagine that the network in Fig. 1B represents one version of an array of possible networks connecting three different oscillators (P, Q, R); and that the edges (i,j,k) and re-entrant loops (p,q,r) represent different connection transfer functions. All 512 possible versions of this re-entrant network, where $R(n) = 2^n D(n)$, can do something interesting. Some versions could be degenerate forms, but needn't be. All must be explored. The overwhelming complexity of the vertebrate retina, even constrained by the simple networks we already know, transcends inference by classical inverse solution methods (Aster et al., 2005) such as physiology or computational modeling. If we consider variations in cell numbers and patterns (Reese, 2008) with time non-stationary synaptic weights, and further include signal conditioning via local cable features, the solution space is effectively infinite. But there is a direct, non-inferential solution: connectomics. Connectomics simply maps the true networks. Though this is a non-trivial computational effort, it is achievable in reasonable time frames with existing technologies (Anderson et al., 2009).

There are arguments against connectomics, nicely summarized and largely rebutted by Morgan and Lichtman (2013), but one theoretical modeling study has particular import for the network diversity argument introduced above. Prinz et al. (2004) produced over 20 million different models of the pyloric rhythm of the crustacean 3-neuron stomatogastic ganglion using seven discrete connections and a wide range of parametric variants for connection features. The authors concluded that over 4 million networks generated proper pyloric rhythms and proposed that, rather than specifying connection features during development or by discrete rules, that some measure of output controlled network parameters and many different biological tunings could suffice. In one sense this further validates the argument that inverse solutions of complex systems (and this is not a complex example at all) create solution spaces too large to parse by physiological methods. One topological motif may serve for many networks which is the "same structure, many functions" argument summarized by Morgan and Lichtman (2013) and exemplified by Prinz et al. (2004). However there are some serious flaws in this argument. First, the ability to create many model solutions does not mean they are all physiologically realizable. Second, even if many solutions can be theoretically realized, this is no proof that they are. Third, and far more important, an example for a single motif that represents an organism's entire architecture is clearly not applicable to complex motifs that are repeated and interconnected to create a processing system. Finally, the notion that topology is thus unimportant is completely invalidated by known retinal architectures, the specific patterns of rod and cone connections with different classes of bipolar cells and horizontal cells, the organization of the primate midget/parvocellular connection stream and much more. The arguments for the high variability of physiological parameters (input resistence, resting potential) in various crustacean models more likely suggests problems with stationarity than variable gene expression. On the whole, the emerging complexities of motifs in retinal networks (Lauritzen et al., 2012a) already argue far more strongly for a "many structure, many function" model than one in which topology is deemed of uncertain value.

4.5. Classification theory and connectomics

The synaptic resolution of electron optical imaging comes at a significant price: the restricted ability to use molecular markers to define cells given the chemical fixation and metallization required to generate electron contrast. In the past, classification of neural cells has largely been based on visual sorting of cell shape visualized by Golgi impregnation or dye injection of cells. This approach has recently been strengthened by the ability to extract single or restricted populations via expression of markers like GFP driven by nominally cell-specific promoters. These approaches, though poorly quantitative so far and only marginally useful for predicting networks, have nevertheless allowed converging estimates of cell diversity in the retina (MacNeil et al., 1999a; b; Rockhill et al., 2002). Further, structural or molecular profiling using cluster analysis (Marc and Cameron, 2003; Marc and Jones, 2002; Marc et al., 1995) support the rich diversity of neurons seen with purely shaped-based analyses. On balance, the number of neuronal classes in the retina is ≈ 70 in mammalians and ≈120–150 non-mammalians.

Other *ad hoc* metrics for cell classification (e.g. cell diameters, Scholl rings, fractals, etc.) have achieved little segmentation power. In the background, however, formal theories of unsupervised multidimensional classification were emerging in remote sensing (Cover and Hart, 1967; MacQueen, 1967). Based on various implementations of clustering algorithms such as the K-means and isodata methods, these approaches showed that the dimensions of a successful classification space should be orthogonal and may be discoverable by using high-dimension sampling.

Recently, classification has been increasingly based on molecular signatures, mostly of cell-restricted proteins. In most cases, however, classification has still been *ad hoc* rather than guided by any formal theory of classification. While it is beyond the scope of this review to develop a full theory of biological types, we can start in the middle of such a theory based on the experimentally robust notion that some molecular signature (proteomic, metabolic, transcriptomic) is a surrogate index for the ultimate class (biologic and mathematic) to which a cell belongs. Given this, some collection of values such as immunoprobe signals can be transformed to N-space vectors and covariance matrices, parsed by classifier algorithms and remapped into human-friendly images (Marc and Cameron, 2003; Marc and Jones, 2002; Marc et al., 1995). Classification itself can be summarized in the clustering relation:

$$S = \operatorname{argmin}_{i=1}^{K} \sum_{n \in S_j} \sum \left| X_n - \mu_j \right|^2 \quad (3)$$

In clustering, x_n represents the molecular signals for n dimensions, i.e. the number of molecular probes. Cells are sorted into K ultimate classes by minimizing S over the classwise sums of data and class centroid (μ) differences. In other words, if the right set of molecular probes exists, all the natural classes of cells can be found. What is the "right" set of probes? Can it be realized? Is there more than one? The key to understanding this approach is the coverage afforded by multivariate signatures. There are over 70 classes of cells in mammalian retina (neurons, glia, microglia, vascular cells) and some are identifiable via surrogate *univariate* molecular tags, e.g. choline acetyltransferase for cholinergic neurons, glutamine synthetase for Müller cells, the calcium binding protein Iba1 for microglia, etc. However, most labs struggle to label their tissues for 2–3 qualitative markers much less 70 quantitative univariate tags, and most protein tags are incompatible with electron imaging.

Univariate tags also have narrow coverage: i.e. one does not know what has *not* been visualized. Conversely, multivariate tags like glutamic acid provide signals in many different cells that differ quantitatively (Kalloniatis et al., 1996; Marc and Jones, 2002; Marc et al., 1990, 1995). By adopting a multivariate strategy such as computational molecular phenotyping (CMP) it is possible to place one or more signals in every cell (Fig. 2) in a TEM dataset (Anderson et al., 2011b, 2009; Lauritzen et al., 2012a), so that even if a biologically ultimate class cannot be extracted for each, at least a very well-defined superclass cohort can be specified. More importantly, it is possible to develop small molecule signature groups that are both robust enough to classify every cell in a cohort and are compliant with TEM (Anderson et al., 2009). Connectomics itself provides additional features for classification via a framework for characterizing all of branches and nodes in a cell and by tracking the shapes and network maps for every cell along with its molecular tags.

4.6. Network notation

Every network is a branched tree through which signals flow, and rarely are networks closed circuits as in electronics. Thus the signaling along chains needs to expressed in some notation and we have devised the following: $>$ denotes high-gain sign-conserving synapses (e.g. mediated by ionotropic glutamate receptors); $>_m$, denotes high-gain sign-inverting synapses (mediated by mGluR6 glutamate receptors), $>_i$, denotes low-gain sign-inverting synapses (ionotropic glycine and GABA receptors), and :: denotes gap junction coupling. High gain transfers are assigned a nominal gain of n and low gain inhibitory transfers are assigned a separate gain of p, based on the idea that most excitatory gains are greater than 1 (Copenhagen et al., 1990; Yang and Wu, 2004) and inhibitory gains are net fractional (Maltenfort et al., 1998; Wu, 1991). Of course none of these values were defined in rabbit retina, but it is likely that the gains of excitation and inhibition are broadly similar across systems and species. Even if that is not correct in all cases, some notation is still required to begin modeling network properties and network chain values can be updated as physiological data improve. Coupling is denoted as c and is presumed to be attenuating. Total chain gains are multiplicative. Thus the chain cone $>_m$ CBb $>$ AC $>_i$ GC has a total gain of n^2p and a net sign-inverting polarity. It is important to understand that each of these parameters is really a vector: a collection of features that collectively determine the total voltage gain between cells. Those features include numbers of synapses, numbers of channels, unitary conductance, transmitter type, receptor subunit composition, receptor and channel kinetics, etc. A combination of connectomics and physiology for every cell type will be required to fully parameterize network models. In the meantime, network chain notation serves as a placeholder.

Disclosure statement

Robert E. Marc is a principal of Signature Immunologics, Inc., manufacturer of antibodies against small molecules used in some of the work described.

Acknowledgments

We thank the National Institutes of Health (EY02576, EY015128, and EY014800), National Science Foundation (0941717), the Thome Foundation, and Research to Prevent Blindness for support. We also thank Shoeb Mohammed for software development; and Hope Morrison, John Vo Hoang, Noah Nelson, and Daniel Emrech for annotation.

References

Amari, S.I., Beltrame, F., Bjaalie, J.G., Dalkara, T., Schutter, E.D., Egan, G.F., Goddard, N.H., Gonzalez, C., Grillner, S., Herz, A., Hoffmann, K.P., Jaaskelainen, I., Koslow, S.H., Lee, S.Y., Matthiessen, L., Miller, P.L., Silva, F.M.D., Novak, M., Ravindranath, V., Ritz, R., Ruotsalainen, U., Sebestra, V., Subramaniam, S., Tang, Y., Toga, A.W., Usui, S., Pelt, J.V., Verschure, P., Willshaw, D., Wrobel, A., 2002. Neuroinformatics: the integration of shared databases and tools towards integrative neuroscience. J. Integr. Neurosci. 1, 117–128.

Anderson, J.R., Grimm, B., Mohammed, S., Jones, B.W., Spaltenstein, J., Koshevoy, P., Tasdizen, T., Whitaker, R., Marc, R.E., 2011a. The Viking Viewer: scalable multiuser annotation and summarization of large connectomics datasets. J. Microsc. 241, 13–28.

Anderson, J.R., Jones, B.W., Watt, C.B., Shaw, M.V., Yang, J.-H., DeMill, D., Lauritzen, J.S., Lin, Y., Rapp, K.D., Mastronarde, D., Koshevoy, P., Grimm, B., Tasdizen, T., Whitaker, R., Marc, R.E., 2011b. Exploring the retinal connectome. Mol. Vis. 17, 355–379.

Anderson, J.R., Jones, B.W., Yang, J.-H., Shaw, M.V., Watt, C.B., Koshevoy, P., Spaltenstein, J., Jurrus, E., UV, Whitaker, R., Mastronarde, D., Tasdizen, T., Marc, R.E., 2009. A computational framework for ultrastructural mapping of neural circuitry. PLoS Biol. 7 (3), e1000074.

Aster, R., Borchers, B., Thurber, C., 2005. Parameter Estimation and Inverse Problems. Academic Press, NY.

Beier, K.T., Borghuis, B.G., El-Danaf, R.N., Huberman, A.D., Demb, J.B., Cepko, C.L., 2013. Transsynaptic tracing with vesicular stomatitis virus reveals novel retinal circuitry. J. Neurosci. 33, 35–51.

Berlanga, M.L., Phan, S., Bushong, E.A., Wu, S., Kwon, O., Phung, B.S., Lamont, S., Terada, M., Tasdizen, T., Martone, M.E., Ellisman, M.H., 2011. Three-dimensional reconstruction of serial mouse brain sections: solution for flattening high-resolution large-scale mosaics. Front. Neuroanat. 5, 17.

Bock, D.D., Lee, W.-C.A., Kerlin, A.M., Andermann, M.L., Hood, G., Wetzel, A.W., Yurgenson, S., Soucy, E.R., Kim, H.S., Reid, R.C., 2011. Network anatomy and in vivo physiology of visual cortical neurons. Nature 471, 177–182.

Bollobás, B., 1998. Modern Graph Theory. Springer, New York, p. 394.

Bourne, J.N., Harris, K.M., 2011. Nanoscale analysis of structural synaptic plasticity. Curr. Opin. Neurobiol. 22, 1–11.

Briggman, K.L., Denk, W., 2006. Towards neural circuit reconstruction with volume electron microscopy techniques. Curr. Opin. Neurobiol. 16, 562–570.

Briggman, K.L., Helmstaedter, M., Denk, W., 2011. Wiring specificity in the direction-selectivity circuit of the retina. Nature 471, 138–188.

Brill, M.H., 1990. Mesopic color matching: some theoretical issues. J. Opt. Soc. Am. A 7, 2048–2051.

Buck, S.L., 1997. Influence of rod signals on hue perception: evidence from successive scotopic contrast. Vis. Res. 37, 1295–3101.

Buck, S.L., 2004. Rod-cone interactions in human vision. In: Chalupa, L.M., Werner, J. (Eds.), Visual Neurosciences. MIT Press, Cambridge, MA, pp. 863–878.

Buck, S.L., Stefurak, D.L., Moss, C., Regal, D., 1984. The time-course of rod-cone interaction. Vis. Res. 24, 543–548.

Calkins, D.J., Sterling, P., 1996. Absence of spectrally specific lateral inputs to midget ganglion cells in primate retina. Nature 381, 613–615.

Calkins, D.J., Sterling, P., 2007. Microcircuitry for two types of achromatic ganglion cell in primate fovea. J. Neurosci. 27, 2646–2653.

Calkins, D.J., Tsukamoto, Y., Sterling, P., 1998. Microcircuitry and mosaic of a blue-yellow ganglion cell in the primate retina. J. Neurosci. 18, 3373–3385.

Copenhagen, D.R., Hemilä, S., Reuter, T., 1990. Signal transmission through the dark-adapted retina of the toad (*Bufo marinus*). Gain, convergence, and signal/noise. J. Gen. Physiol. 95, 717–732.

Cover, T., Hart, P., 1967. Nearest neighbor pattern classification. IEEE Trans. Inf. Theory 13, 21–27.

Denk, W., Horstmann, H., 2004. Serial block-face scanning electron microscopy to recon-struct three-dimensional tissue nanostructure. PLoS Biol. 2, e329.

DeVries, S.E., Baccus, S.A., Meister, M., 2011. The projective field of a retinal amacrine cell. J. Neurosci. 31, 8595–8604.

Diestel, R., 2010. Graph Theory. Springer-Verlag, Heidelberg, p. 41.

Dowling, J.E., 1968. Synaptic organization of the frog retina: an electron microscopic analysis comparing the retinas of frogs and primates. Proc. R. Soc. Lond. B Biol. Sci. 170, 205–228.

Dowling, J.E., Boycott, B.B., 1966. Organization of the primate retina: electron microscopy. Proc. R. Soc. Lond. B Biol. Sci. 166, 80–111.

Duda, R.O., Hart, P.E., Stork, D.G., 2001. Pattern Classification. Wiley, NY, 654 p.

Dumitrescu, O.N., Pucci, F.G., Wong, K.Y., Berson, D.M., 2009. Ectopic retinal ON bipolar cell synapses in the OFF inner plexiform layer: contacts with dopaminergic amacrine cells and melanopsin ganglion cells. J. Comp. Neurol. 517, 226–244.

Famiglietti, E.V.J., 1981. Functional architecture of cone bipolar cells in mammalian retina. Vis. Res. 21, 1559–1563.

Famiglietti, E.V.J., Kolb, H., 1975. A bistratified amacrine cell and synaptic circuitry in the inner plexiform layer of the retina. Brain Res. 84, 293–300.

Fiala, J.C., 2005. Reconstruct: a free editor for serial section microscopy. J. Microsc. 218, 52–61.

Frumkes, T.E., Eysteinsson, T., 1988. The cellular basis for suppressive rod-cone interaction. Vis. Neurosci. 1, 263–273.

Gaietta, G., Deerinck, T.J., Adams, S.R., Bouwer, J., Tour, O., Laird, D.W., Sosinsky, G.E., Tsien, R.Y., Ellisman, M.H., 2002. Multicolor and electron microscopic imaging of connexin trafficking. Science 296, 503–507.
Goldberg, S.H., Frumkes, T.E., Nygaard, R.W., 1983. Inhibitory influence of unstimulated rods in the human retina: evidence provided by examining cone flicker. Science 221, 180–182.
Gollisch, T., Meister, M., 2008. Rapid neural coding in the retina with relative spike latencies. Science 319, 1108–1111.
Google, 2010. KML Reference – KML – Google Code. Google, Inc.
Guo, J.L., Nagarajah, R., Banati, R.B., Bennett, M.R., 2009. Glutamate induces directed chemotaxis of microglia. Eur. J. Neurosci. 29, 1108–1118.
Han, Y., Massey, S., 2005. Electrical synapses in retinal ON cone bipolar cells: subtype-specific expression of connexins. Proc. Natl. Acad. Sci. U. S. A. 102, 13313–13318.
Harary, F., Palmer, E.M., 1973. Graphical Enumeration. Academic Press, New York.
Helmstaedter, M., Briggman, K.L., Turaga, S.C., Jain, V., Seung, H.S., Denk, W., 2013. Connectomic reconstruction of the inner plexiform layer in the mouse retina. Nature 500, 168–174.
Hoffmann, C., Gaietta, G., Zürn, A., Adams, S.R., Terrillon, S., Ellisman, M.H., Tsien, R.Y., Lohse, M.J., 2010. Fluorescent labeling of tetracysteine-tagged proteins in intact cells. Nat. Protoc. 5, 1666–1677.
Hoshi, H., Liu, W.-L., Massey, S.C., Mills, S.L., 2009. ON inputs to the OFF layer: bipolar cells that break the stratification rules of the retina. J. Neurosci. 29, 8875–8883.
Hsueh, H.A., Molnar, A., FS, W., 2008. Amacrine-to-amacrine cell inhibition in the rabbit retina. J. Neurophysiol. 100, 2077–2088.
Hu, E.H., Bloomfield, S.A., 2003. Gap junctional coupling underlies the short-latency spike synchrony of retinal alpha ganglion cells. J. Neurosci. 23, 6768–6777.
Huberman, A.D., Niell, C.M., 2011. What can mice tell us about how vision works? Trends Neurosci. 34, 464–473.
Jeong, W., Beyer, J., Hadwiger, M., Blue, R., Law, C., Vazquez, A., Reid, C., Lichtman, J., Pfister, H., 2010. SSECRETT and NeuroTrace: interactive visualization and analysis tools for large-scale neuroscience datasets. IEEE Comp. Graph. Appl. 30, 58–70.
Jones, B.W., Kondo, M., Terasaki, H., Watt, C.B., Rapp, K., Anderson, J., Lin, Y., Shaw, M.V., Yang, J.-H., Marc, R.E., 2011. Retinal degenerative disease and remodeling in a large eye model. J. Comp. Neurol. 519, 2713–2733.
Jones, B.W., Watt, C.B., Frederick, J.M., Baehr, W., Chen, C.K., Levine, E.M., Milam, A.H., LaVail, M.M., Marc, R.E., 2003. Retinal remodeling triggered by photoreceptor degenerations. J. Comp. Neurol. 464, 1–16.
Kalloniatis, M., Marc, R.E., Murry, R.F., 1996. Amino acid signatures in the primate retina. J. Neurosci. 16, 6807–6829.
Kamasawa, N., Furman, C.S., Davidson, K.G., Sampson, J.A., Magnie, A.R., Gebhardt, B.R., Kamasawa, M., Yasumura, T., Zumbrunnen, J.R., Pickard, G.E., Nagy, J.I., Rash, J.E., 2006. Abundance and ultrastructural diversity of neuronal gap junctions in the OFF and ON sublaminae of the inner plexiform layer of rat and mouse retina. Neuroscience 142, 1093–1117.
Karp, R.M., 1972. Reducibility among combinatorial problems. In: Miller, R.E., Thatcher, J.W. (Eds.), Complexity of Computer Computations. Plenum, New York, pp. 85–103.
Kleinfeld, D., Bharioke, A., Blinder, P., Bock, D.D., Briggman, K.L., Chklovskii, D.B., Denk, W., Helmstaedter, M., Kaufhold, J.P., Lee, W.C., Meyer, H.S., Micheva, K.D., Oberlaender, M., Prohaska, S., Reid, R.C., Smith, S.J., Takemura, S., Tsai, P.S., Sakmann, B., 2011. Large-scale automated histology in the pursuit of connectomes. J. Neurosci. 31, 16125–16138.
Klug, K., Herr, S., Ngo, I.T., Sterling, P., Schein, S., 2003. Macaque retina contains an S-cone OFF midget pathway. J. Neurosci. 23, 9881–9887.
Knott, G., Marchman, H., Wall, D., Lich, B., 2008. Serial section scanning electron microscopy of adult brain tissue using focused ion beam milling. J. Neurosci. 28, 2959–2964.
Kolb, H., Famiglietti, E.V., 1974a. Rod and cone pathways in the inner plexiform layer of cat retina. Science 186, 47–49.
Kolb, H., Famiglietti, E.V.J., 1974b. Rod and cone pathways in the retina of the cat. Invest Ophthal 15, 935–946.
Kolb, H., Nelson, R., 1993. OFF-alpha and OFF-beta ganglion cells in cat retina: II. Neural circuitry as revealed by electron microscopy of HRP stains. J. Comp. Neurol. 329, 85–110.
Korkhov, V.M., Zuber, B., 2009. Direct observation of molecular arrays in the organized smooth endoplasmic reticulum. BMC Cell Biol. 10, 59–68.
Lange, G., Denny, N., Frumkes, T.E., 1997. Suppressive rod-cone interactions: evidence for separate retinal (temporal) and extraretinal (spatial) mechanisms in achromatic vision. J. Opt. Soc. Am. A Opt. Image Sci. Vis. 14, 2487–2498.
Lauritzen, J.S., Anderson, J.R., Jones, B.W., Watt, C.B., Mohammed, S., Hoang, J.V., Marc, R.E., 2012a. ON cone bipolar cell axonal synapses in the OFF inner plexiform layer of the rabbit retina. J. Comp. Neurol. 521, 977–1000.
Lauritzen, J.S., Hoang, J.V., Sigulinsky, C., Jones, B.W., Anderson, J.R., Watt, C.B., Mohammed, S., Marc, R.E., 2013. Tiered cross-class bipolar cell gap junctional coupling in the rabbit retina. Invest. Ophthal. 54, 1754.
Lauritzen, J.S., Jones, B.W., Watt, C.B., Mohammed, S., Anderson, J.R., Marc, R.E., 2012b. Diffusely-stratified OFF cone bipolar cell inputs to amacrine cells in the ON inner plexiform layer. Invest. Ophthalmol. Vis. Sci. 53, 3159.
Liang, Z., Freed, M.A., 2012. Cross inhibition from ON to OFF pathway improves the efficiency of contrast encoding in the mammalian retina. J. Neurophysiol. 108, 2679–2688.
Liang, J., Takeuchi, H., Jin, S., Noda, M., Li, H., Doi, Y., Kawanokuchi, J., Sonobe, Y., Mizuno, T., Suzumura, A., 2010. Glutamate induces neurotrophic factor production from microglia via protein kinase C pathway. Brain Res. 1322, 8–23.
Liang, Z., Freed, M.A., 2010. The ON pathway rectifies the OFF pathway of the mammalian retina. J. Neurosci., 5533–5543.
Lichtman, J.W., Smith, S.J., 2008. Seeing circuits assemble. Neuron 60, 441–448.
MacNeil, M.A., Heussy, J.K., Dacheux, R.F., Raviola, E., Masland, R.H., 1999a. The population of amacrine cells in a mammalian retina. Invest. Ophthalmol. Vis. Sci. 40, 437.
MacNeil, M.A., Heussy, J.K., Dacheux, R.F., Raviola, E., Masland, R.H., 1999b. The shapes and numbers of amacrine cells: matching of photofilled with golgi-stained cells in the rabbit retina and comparison with other mammalian species. J. Comp. Neurol. 413, 305–326.
MacQueen, J., 1967. Some methods for classification and analysis of multivariate observations. Proc 5th Berkeley Symposium, 281–297.
Maltenfort, M.G., Heckman, C.J., Rymer, W.Z., 1998. Decorrelating actions of Renshaw interneurons on the firing of spinal motoneurons within a motor nucleus: a simulation study. J. Neurophysiol. 80, 309–323.
Marc, R.E., 2010. Synaptic organization of the retina. In: Levin, L.A., Nilsson, S.F.E., Ver Hoeve, J., Wu, S.M., Kaufman, P.L., Alm, A. (Eds.), Adler's Physiology of the Eye. Elsevier, pp. 443–458.
Marc, R.E., Cameron, D.A., 2003. A molecular phenotype atlas of the zebrafish retina. J. Neurocytol. 30, 593–654.
Marc, R.E., Jones, B.W., 2002. Molecular phenotyping of retinal ganglion cells. J. Neurosci. 22, 412–427.
Marc, R.E., Jones, B.W., Lauritzen, J.S., Watt, C.B., Anderson, J.R., 2012a. Building retinal connectomes. Curr. Opin. Neurobiol. 22, 568–574.
Marc, R.E., Lauritzen, J.S., Jones, B.W., Watt, C.B., Anderson, J.R., 2012b. The synaptic basis of rod-cone pathway interactions. Invest. Ophthal. 53, 6324.
Marc, R.E., Liu, W., 2000. Fundamental GABAergic amacrine cell circuitries in the retina: nested feedback, concatenated inhibition, and axosomatic synapses. J. Comp. Neurol. 425, 560–582.
Marc, R.E., Liu, W.L., Kalloniatis, M., Raiguel, S.F., van Haesendonck, E., 1990. Patterns of glutamate immunoreactivity in the goldfish retina. J. Neurosci. 10, 4006–4034.
Marc, R.E., Murry, R.F., Basinger, S.F., 1995. Pattern recognition of amino acid signatures in retinal neurons. J. Neurosci. 15, 5106–5129.
Marc, R.E., Vazquez-Chona, F., Hoang, J.V., Sigulinsky, C., Watt, C.B., Jones, B.W., Anderson, J.R., Lauritzen, J.S., 2013. Pure feedforward amacrine cells. Invest. Ophthal. 54, 2503.
Marcus, D.S., Harwell, J., Olsen, T., Hodge, M., Glasser, M.F., Prior, F., Jenkinson, M., Laumann, T., Curtiss, S.W., Van Essen, D.C., 2011. Informatics and data mining tools and strategies for the human connectome project. Front. Neuroinform. 5, 4.
Massey, S.C., 2008. Circuit functions of gap junctions in the mammalian retina. In: Masland, R.H., Albright, T. (Eds.), The Senses. Academic Press, pp. 457–472.
Mastronarde, D.N., 2005. Automated electron microscope tomography using robust prediction of specimen movements. J. Struct. Biol. 152, 36–51.
Micheva, K.D., Bruchez, M.P., 2011. The gain in brain: novel imaging techniques and multiplexed proteomic imaging of brain tissue ultrastructure. Curr. Opin. Neurobiol. 22, 94–100.
Micheva, K.D., Busse, B., Weiler, N.C., O'Rourke, N., Smith, S.J., 2010. Single-synapse analysis of a diverse synapse population: proteomic imaging methods and markers. Neuron 68, 639–653.
Micheva, K.D., Smith, S.J., 2007. Array tomography: a new tool for imaging the molecular architecture and ultrastructure of neural circuits. Neuron 55, 25–36.
Middleton, T.P., Protti, D.A., 2011. Cannabinoids modulate spontaneous synaptic activity in retinal ganglion cells. Vis. Neurosci. 28, 393–402.
Mikula, S., Trotts, I., Stone, J.M., Jones, E.G., 2007. Internet-enabled high-resolution brain mapping and virtual microscopy. Neuroimage 35 (1), 9–15.
Morgan, J.L., Lichtman, J.W., 2013. Why not connectomics. Nat. Methods 10, 494–500.
Oberlaender, M., Boudewijns, Z.S., Kleele, T., Mansvelder, H.D., Sakmann, B., de Kock, C.P., 2011. Three-dimensional axon morphologies of individual layer 5 neurons indicate cell type-specific intracortical pathways for whisker motion and touch. Proc. Natl. Acad. Sci. U. S. A 108, 4188–4193.
Pocock, J.M., Kettenmann, H., 2007. Neurotransmitter receptors on microglia. Trends Neurosci. 30, 527–535.
Prinz, A.A., Bucher, B., Marder, E., 2004. Similar network activity from disparate circuit parameters. Nat. Neurosci. 7, 1345–1352.
Reese, B.E., 2008. Mosaics, tiling and coverage by retinal neurons. In: Masland, R.H., Albright, T. (Eds.), The Senses. Academic Press, San Diego, pp. 439–456.
Rivlin-Etzion, M., Zhou, K., Wei, W., Elstrott, J., Nguyen, P.L., Barres, B.A., Huberman, A.D., Feller, M.B., 2011. Transgenic mice reveal unexpected diversity of on-off direction-selective retinal ganglion cell subtypes and brain structures involved in motion processing. J. Neurosci. 31, 8760–8769.
Rockhill, R.L., Daly, F.J., MacNeil, M.A., Brown, S.P., Masland, R.H., 2002. The diversity of ganglion cells in a mammalian retina. J. Neurosci. 22, 3831–3843.
Sherry, D.M., Yazulla, S., 1993. Goldfish bipolar cells and axon terminal patterns: a golgi study. J. Comp. Neurol. 329, 188–200.
Shu, X., Lev-Ram, V., Deerinck, T.J., Qi, Y., Ramko, E.B., Davidson, M.W., Jin, Y., Ellisman, M.H., Tsien, R.Y., 2011. A genetically encoded tag for correlated light and electron microscopy of intact cells, tissues, and organisms. PLoS Biol. 9, e1001041.

Snapp, E.L., Hegde, R.S., Francolini, M., Lombardo, F., Colombo, S., Pedrazzini, E., Borgese, N., Lippincott-Schwartz, J., 2003. Formation of stacked ER cisternae by low affinity protein interactions. J. Cell Biol. 163, 257–269.
Sporns, O., Tononi, G., Kötter, R., 2005. The human connectome: a structural description of the human brain. PLoS Comput. Biol. 1, e42.
Stabell, B., Stabell, U., 1998. Chromatic rod-cone interaction during dark adaptation. J. Opt. Soc. Am. A Opt. Image Sci. Vis. 15, 2809–2815.
Stabell, B., Stabell, U., 2002. Effects of rod activity on color perception with light adaptation. J. Opt. Soc. Am. A Opt. Image Sci. Vis. 19, 1249–1258.
Stevens, J.K., Davis, T.L., Friedman, N., Sterling, P., 1980. A systematic approach to reconstructing microcircuitry by electron microscopy of serial sections. Brain Res. 2, 265–293.
Strettoi, E., Raviola, E., Dacheux, R.F., 1992. Synaptic connections of the narrow-field, bistratified rod amacrine cell (AII) in the rabbit retina. J. Comp. Neurol. 325, 152–168.
Tasdizen, T., Koshevoy, P., Grimm, B., Anderson, J.R., Jones, B.W., Whitaker, R., Marc, R.E., 2010. Automatic mosaicking and volume assembly for high-throughput serial-section transmission electron microscopy. J. Neurosci. Methods 193, 132–144.
Thomas, L.P., Buck, S.L., 2006. Foveal and extra-foveal influences on rod hue biases. Vis. Neurosci. 23, 539–542.
Trezona, P.W., 1970. Rod participation in the 'blue' mechanism and its effect on colour matching. Vis. Res. 10, 317–332.
Trezona, P.W., 1973. The tetrachromatic colour match as a colorimetric technique. Vis. Res. 13, 9–25.
van den Heuvel, M.P., Sporns, O., 2011. Rich-Club organization of the human connectome. J. Neurosci. 31, 15775–15786.
Vaney, D.I., 2004. Retinal amacrine cells. In: Chalupa, L.M., Werner, J. (Eds.), The Visual Neurosciences. MIT Press, Cambridge, MA, pp. 395–409.
Van Essen, D.C., Glasser, M.F., Dierker, D.L., Harwell, J., Coalson, T., 2011. Parcellations and hemispheric asymmetries of human cerebral cortex analyzed on surface-based atlases. Cereb. Cortex 22, 2241–2262.
Vaney, D.I., Weiler, R., 2000. Gap junctions in the eye: evidence for heteromeric, heterotypic and mixed-homotypic interactions. Brain Res. – Brain Res. Rev. 32 (1), 115–120.
Voigt, T., Wassle, H., 1987. Dopaminergic innervation of AII amacrine cells in mammalian retina. J. Neurosci. 7 (12), 4115–4128.
Völgyi, B., Pan, F., Paul, D.L., Wang, J.T., Huberman, A.D., Bloomfield, S.A., 2013. Gap junctions are essential for generating the correlated spike activity of neighboring retinal ganglion cells. PLoS One 8, e69426.
Wake, H., Moorhouse, A.J., Jinno, S., Kohsaka, S., Nabekura, J., 2009. Resting microglia directly monitor the functional state of synapses in vivo and determine the fate of ischemic terminals. J. Neurosci. 29, 3974–3980.
Wake, H., Moorhouse, A.J., Miyamoto, A., Nabekura, J., 2013. Microglia: actively surveying and shaping neuronal circuit structure and function. Trends Neurosci. 36, 209–217.
Werblin, F.S., 2010. Six different roles for crossover inhibition in the retina: correcting the nonlinearities of synaptic transmission. Vis. Neurosci. 27, 1–8.
Werblin, F.S., 2011. The retinal hypercircuit: a repeating synaptic interactive motif underlying visual function. J. Physiol. 589, 3691–3702.
Witkovsky, P., Dowling, J.E., 1969. Synaptic relationships in the plexiform layers of carp retina. Z. Zellforsch. Mikrosk. Anat. 100, 60–82.
Wu, S.M., 1991. Input-output relations of the feedback synapse between horizontal cells and cones in the tiger salamander retina. J. Neurophysiol. 65, 1197–1206.
Xie, X., Schnieder, M.C., Sánchez-Sinencio, E., Embabi, S.H.K., 1999. Sound design of low power nested transconductance-capacitance compensation amplifiers. IEEE Electron. Lett. 35, 956–958.
Xin, D., Bloomfield, S.A., 1997. Tracer coupling pattern of amacrine and ganglion cells in the rabbit retina. J. Comp. Neurol. 383, 512–528.
Yang, X.L., Wu, S.M., 2004. Signal transmission from cones to amacrine cells in dark- and light-adapted tiger salamander retina. Brain Res. 1029, 155–161.
Yazulla, S., 2008. Endocannabinoids in the retina: from marijuana to neuroprotection. Prog. Retin. Eye Res. 27, 501–526.